ABSTRACT

VETRENO, JOANNA RUTH. Analytic Models for Acoustic Wave Propagation in Air. (Under the direction of Dr. Michael B. Steer).

Ultrasound waves have been used for imaging purposes for many years. However, a liquid interface has always been necessary between the transducer and the object being imaged due to a high mechanical resistance at the air-transducer interface. Recent advances in transducers have made it possible to omit the liquid interface, allowing imaging to be done through air interfaces. Because this is a relatively new field, research into ultrasound propagation in air is very limited. A comprehensive model of how an ultrasound wave propagates through air would expedite the study of air-coupled ultrasound for imaging. This thesis presents a mathematical model of two-dimensional linear acoustic wave propagation in air. The model takes as input the frequency and amplitude of an acoustic signal and outputs the pressure field over varying longitudinal and lateral distances from the source. The benefits of a mathematical model over a finite element model are first discussed, then the mathematical model for acoustic propagation in air is developed using both computer simulations and physical experiments in an anechoic chamber. Results are presented and compared to experimental data to confirm the validity of the mathematical model.

Analytic Models for Acoustic Wave Propagation in Air

By

JoAnna R. Vetreno

A thesis submitted to the Graduate Faculty of
North Carolina State University
in partial fulfillment of the
requirements for the Degree of
Master of Science

Electrical Engineering

Raleigh, NC

2007

Approved by:

_____	_____
Professor Michael B. Steer Chair of Advisory Committee	Professor Hamid Krim

_____

Professor Kevin Gard

DEDICATION

To

Mike Adelson
Omar Elshahawi
Yale Goodman
Tim Kaefer
Joseph Thurakal

There from the beginning

Sue Hoyt
&
Carmen Kampf

For introducing me to the joy of physics and calculus,
from which I never looked back

BIOGRAPHY

JoAnna Vetreno was born on the 12th of August, 1983 along with a twin brother Michael. She grew up in Oakland, a small town in northern New Jersey. She received her Bachelor of Science (B.S.) degree in Electrical and Computer Engineering from Lafayette College, located in Easton, Pennsylvania, in 2006. In the fall of 2006 she began her graduate studies in the Electrical and Computer Engineering Department at North Carolina State University in Raleigh, NC, focusing on analog circuit design. She is a member of the Institute of Electrical and Electronics Engineers (IEEE), Eta Kappa Nu (HKN), the electrical engineering honor society, and Sigma Xi, the scientific research society. Since the spring of 2005, she has been working for the SIAMES group under the tutelage of Dr. Michael B. Steer. Her project involves the modeling of ultrasound propagation through air in the use of object characterization and imaging.

TABLE OF CONTENTS

LIST OF TABLES

LIST OF FIGURES

LIST OF SYMBOLS

Symbol	Unit	Description
a	unit less	Linear scaling factor
$\ddot{a}(x,t)$	m/s^2	Particle acceleration
A	m	Oscillation amplitude
b	unit less	Nonlinear restoring force
B	Pa	Adiabatic bulk modulus
B/A	unit less	parameter of nonlinearity
c	m/s	Speed of wave propagation
c_o	m/s	Speed of sound propagation
$c_{\wp}$	J/(kg*K)	Specific heat at constant pressure
CFL	unit less	Wave distance per time step
f_o	Hz	Source frequency
f_y	N	Force element in the y direction
F	N	Force
F_r	N	Viscous friction force
h	m	Maximum mesh element size
I	W/m^2	Intensity
I_{ref}	W/m^2	Reference intensity
$I(t)$	W/m^2	Instantaneous intensity
IL	dB	Intensity level
k	rad/m	Wave number
l	m	Length of source
L	unit less	Second-order Lagrangian
m	kg	Mass
M_o	unit less	Amplitude mach number
N	unit less	Resolution parameter
p'	Pa	Perturbation pressure
p_o	Pa	Equilibrium pressure
P_o	Pa	Initial pressure amplitude
P_{REF}	Pa	Reference pressure
P_{RMS}	Pa	Root mean square pressure
$p(x,t)$	Pa	Acoustic pressure
Psq	Pa^2	Square of instantaneous pressure
R	m	Distance from source
R_m	Kg/s	Mechanical resistance

Symbol	Unit	Description
s	N/m	Spring constant
s_c	unit less	Condensation
SPL	dB	Sound pressure level
t	s	Time
t_{MAX}	s	Limiting time step size
T	s	Period of a wave
T_s	N	Tension
u_o	m/s	Initial velocity
$\vec{u}(x,t)$	m/s	Particle velocity
x_d	m	Discontinuity distance
x_o	m	Initial displacement
$\vec{x}(x,t)$	m	Particle displacement
Z_o	Pa*s/m	Specific acoustic impedance
a	Np/m	Attenuation coefficient
$\overline{a}$	dB/m	Attenuation coefficient in decibels
a_d	Np/m	Damping coefficient
a_k	Np/m	Thermal attenuation
a_v	Np/m	Viscous attenuation
b	unit less	Coefficient of nonlinearity
g	unit less	Ratio of specific heats
d	m^2/s	Diffusivity of sound
h	Pa*s	Shear viscosity coefficient
h_B	Pa*s	Coefficient of bulk viscosity
k	W/(m*K)	Thermal conductivity
l	m	Wavelength
r	kg/m^3	Instantaneous density
r_L	kg/m	Linear density
r_o	kg/m^3	Equilibrium density
r'	kg/m^3	Perturbation density
t	s	Retarded time
f	rad	Phase
Ψ	m^2/s	Velocity potential
w_d	rad/s	Damped natural frequency
w_o	rad/s	Radial frequency

Chapter 1 Introduction

1.1 Motivation

Using high frequency acoustics (ultrasound) for imaging, non-destructive testing, and other purposes is a common and well understood practice. However, to date all methods of using ultrasound for imaging have relied on a fluid coupling between the transducer and the media being tested or imaged. There is increasing interest in the use of noncontact, gas coupled ultrasound in imaging for many reasons. It is simpler, lower in cost, and, by removing the usual fluid coupling requirement, allows imaging of objects a distance away and in applications where a liquid coupler is impractical.

The use of ultrasonic acoustics in biomedical and underwater imaging and non-destructive testing works by sending ultrasound waves into a medium through a liquid interface, which are then scattered and reflected back to a receiver. The scattered and reflected waves are processed and information is then extracted which can describe material properties as well as generate images of the interior of the medium. Some well known examples of this are obstetric ultrasound, medical sonography, nondestructive materials testing, and underwater sonic imaging used by ships, submarines, and even fishermen.

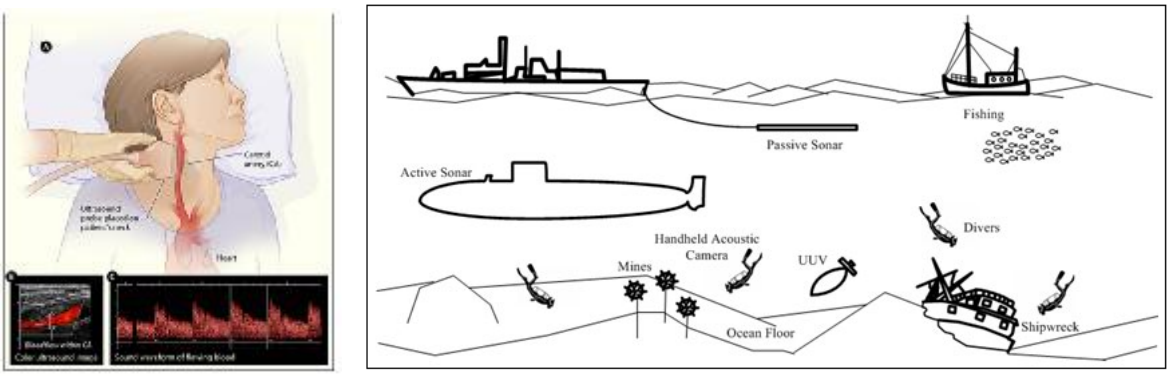

Figure 1.1: Medical sonography of the carotid artery (left [1]) and underwater sonic imaging (right [2])

Using ultrasound for imaging in biomedical and underwater applications is a fairly well understood and well researched phenomenon. However, it relies on a transducer-liquid-media interfacing for its functionality. Of great interest lately is the possibility of using ultrasound for imaging without the need of the liquid interface between the transducer and the media being tested. Previously, this field had been limited by the high mechanical impedance mismatch of a transducer-air interface, causing low coupling and high loss of the acoustic wave into the air. However, recent advances in the generation of transducers have made this problem less significant, opening the door to ultrasound testing with transducer-air-object interfacing.

Using ultrasound in air for imaging is a relatively new field. It relies on inherent nonlinearities in air that affect the propagation of the ultrasonic wave, causing mixing of the frequencies being propagated. This nonlinear effect only becomes significant at high frequencies, which is why the acoustic wave used in imaging must be in the ultrasound frequency range (20k Hz and above). Research into this field is still young, with most of

the studies focusing on the various transducer varieties, how to design them for good air coupling, and how properties of air affect acoustic propagation.

An immense body of research exists on the characterization of ultrasound activity in liquid and solid media, but there is surprisingly little on the propagation of ultrasound in gases, given the possibilities for the field. Currently, the majority of work has been examinations of how the atmosphere decays the acoustic wave and studies of the design and characterization of the transducers that generate the ultrasound. What is lacking in the research of air coupled ultrasound is a fast computation model that can predict the propagation field in air. Such a model would make it easier to predict ultrasound interactions with and reflections from objects based on initial pressure level and propagation distance information.

1.2 Contribution

It has been shown that the frequency response of one or two ultrasonic tones mixing together as they propagate through air and then impinging on an object can be used to determine characteristics of the object such as density, size, hollowness, material, etc. It is thus beneficial to study and characterize the nonlinear propagation and spread of a single acoustic tone through the atmosphere. However, difficulties arise when modeling this phenomenon due to the small wavelength of ultrasound propagation in air. Because the wavelength of an ultrasound wave is so small (on the order of millimeters), finite element modeling programs used to generate the model require higher resolution than can be

supported by the computers in existence today. This requirement severely limits the size of the model that can be created and greatly increases computation time, to a point where the model is no longer useful.

It is therefore useful to come up with a mathematical model of the wave propagation, which can significantly reduce computation time when studying wave interaction with objects and air. The goal of such a model (Figure 1-2) is to predict the spread and propagation of an ultrasound wave given only its initial amplitude and frequency.

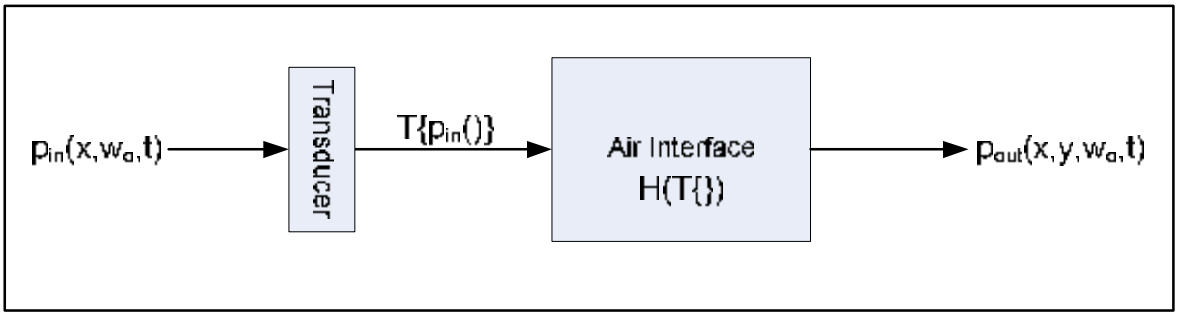

Figure 1.2: Block diagram of the mathematical model for predicting the two dimensional propagation characteristic of ultrasound in the atmosphere. Given an initial amplitude and frequency, the model computes the 2D wave field.

This thesis examines the propagation of a pure ultrasonic acoustic tone in air and presents a mathematical model that describes the phenomenon.

1.3 Thesis Organization

Chapter 2 gives a detailed review of the basic physical phenomena and equations that govern acoustic propagation, both linear and nonlinear. Chapter 3 examines pre-existing research in the field and then outlines the development of this thesis topic. Chapter 4 presents an experimental model and a computer model and verifies the accuracy of those models. Results from these models will be used to generate the mathematical model. Chapter 5 presents experimental data from the models and then details the development of the mathematical model for acoustic propagation in the atmosphere. Chapter 6 concludes the work done and gives some guidelines for future work.

REFERENCES

[1] Image taken from the National Heart Lung and Blood Institute, Diseases and Conditions Index website on November 20th, 2007. http://www.nhlbi.nih.gov/health/dci/Diseases/cu/cu_all.html

[2] Image taken from the Khuri-Yakub Ultrasonics Group website on November 20th, 2007. http://www-kyg.stanford.edu/khuriyakub/opencms/en/research/ultrasonic/Sonar/index.html

Chapter 2 Physical Background

2.1 Introduction

When ultrasound is used for imaging, one or two directional tones are transmitted via a transducer into the air, after which reflections of the sound beams are recorded and used to determine various properties of the object under examination. Therefore, of interest in this research is the propagation of single tone directed ultrasound. This chapter presents a detailed background on acoustic propagation but focuses on the propagation of single tone plane waves. Before delving into the topic of ultrasonic acoustic propagation, it is beneficial to review the basics of particle oscillation that lead to the transmission of acoustic waves through a medium. This chapter gives a general review of the physical equations that govern both linear and nonlinear wave motion through the air, and presents the partial differential equation that describes the pressure variation of a medium as a single frequency acoustic wave propagates. If the reader already has a strong background in wave motion then they are encouraged to jump ahead to the derivation of the damped linear wave equation (Section 2.5.2) and the nonlinear Westervelt equation (Section 2.7) which are the most pertinent equations for this thesis.

2.2 Fundamentals of Acoustic Propagation

Acoustic waves are pressure disturbances in the form of vibrational waves that propagate through a compressible medium. These vibrational waves displace the molecules of the medium from their quiescent point, after which a restoring elastic force pulls the

molecules back. This elastic force, along with inertia, causes the molecules to oscillate, allowing acoustic waves to propagate. The oscillatory motion is analogous to the motion of a spring when displaced from its rest position, while the propagation of the wave itself is analogous to the movement of a wave down a piece of string. The most well known acoustic waves are those of sound. The audible frequency range for an average person is 20 Hz to 20k Hz; the range above the audible (greater than 20k Hz) is called the ultrasonic region, and the range below the audible (less than 20 Hz) is called the infrasonic region.

This thesis will concern itself only with acoustic waves in air, and the assumption is made that the waves are plane waves. To be planar means that each acoustic variable has constant amplitude on any given plane perpendicular to the direction of propagation. This assumption greatly simplifies the derivations of acoustic equations and relationships, and is valid in most experimental situations because wave fronts of any divergent wave in a homogeneous medium become approximately planar when sufficiently far from the source. Sufficiently far from the source means that the wave is in the far field, as opposed to the near field. The separation distance that designates far from near is given by

$$R >> \frac{l^2}{l} \qquad \text{(Equation 2-1)}$$

where l is the length of the source, l is the wavelength of the wave and R is the measuring distance from the source [1].

Acoustic plane waves in air are longitudinal, which means that the particle displacement caused by the vibrational disturbance is in the direction of propagation

(Figure 2.1). This produces adjacent regions of compression and rarefaction of the air particles as the wave moves.

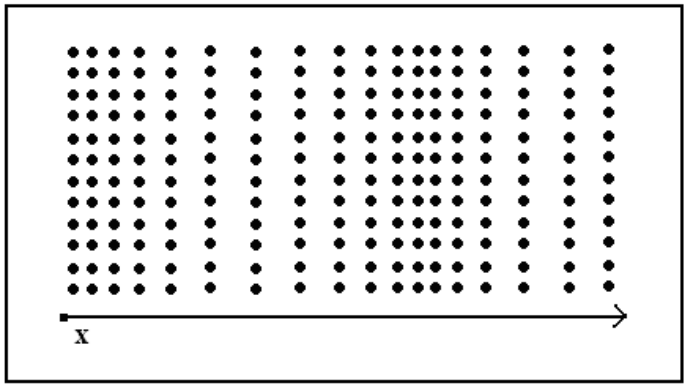

Figure 2.1: Compression and rarefaction of air particles due to longitudinal wave propagation through a medium.

Speaking of wave propagation in terms of air particles is more accurate that air molecules, because in general molecules move through a medium in erratic and unpredictable manners. Instead, a particle of the medium is defined which is small enough to assume that all physical quantities are constant across the particle but large enough to assume that the random motion of the molecules within the particle average out to uniform.

2.3 Basic Oscillatory Motion

2.3.1 Ideal oscillation

The oscillatory motion of air particles produced by acoustic propagation can most easily be described by examining the motion of a mass on a spring, shown in Figure 2.2.

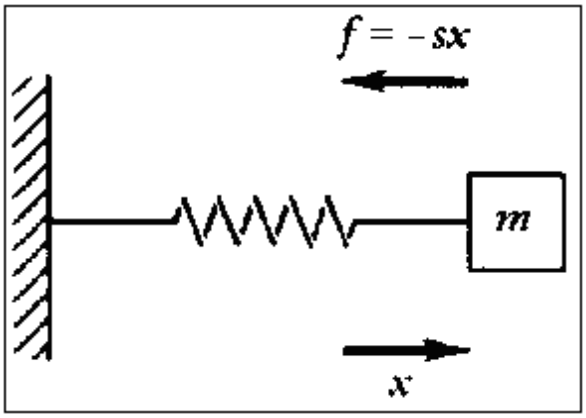

Figure 2.2: Diagram of a mass on a spring [2]

The mass is analogous to a single air particle and the spring is analogous to the previously described restoring elastic forces. When the mass m in kilograms (kg) is displaced in the positive x direction in meters (m), a restoring force F in newtons (N) can be defined by the equation

$$F = -s * x \qquad \text{(Equation 2-2)}$$

where s is the spring constant of the spring in N/m. Combining this with the general equation of motion

$$F = m * \frac{d^2x}{dt^2} \qquad \text{(Equation 2-3)}$$

where $\frac{d^2x}{dt^2}$ is the acceleration of the mass, yields the differential equation

$$\frac{d^2x}{dt^2} + \frac{s}{m}x = 0 \qquad \text{(Equation 2-4)}$$

This differential equation has the general solution

$$x(t) = A_1 \cos(w_o t) + A_2 \sin(w_o t) \qquad \text{(Equation 2-5)}$$

where A_1 and A_2 are arbitrary constants defined by initial conditions and w_o is the natural angular frequency, defined by $\sqrt{s/m}$. The general solution can be transformed into a more useful solution by defining $A_1 = A\cos(f)$ and $A_2 = -A\sin(f)$ where A is the motion amplitude and f is the initial phase angle, which when substituted into Equation 2-5 gives the final solution

$$\mathbf{v}\ddot{x}(t) = A\cos(w_o t + f) \qquad \text{(Equation 2-6)}$$

Definitions of A and f can be derived by examining the initial conditions of the system. If the spring at time $t = 0$ has a position x_o with an initial speed u_o, then substitution and differentiation shows that

$$A = \sqrt{x_o^2 + (u_o / w_o)^2} \qquad \text{(Equation 2-6a)}$$

$$f = \tan^{-1}\left(\frac{-u_o}{w_o x_o}\right) \qquad \text{(Equation 2-6b)}$$

Equations for velocity and acceleration of the particle can be obtained by successive differentiation of Equation 2-6:

$$\mathbf{v}\dot{u}(t) = -w_o A\sin(w_o t + f) \qquad \text{(Equation 2-7)}$$

$$\mathbf{v}\ddot{a}(t) = -w_o^2 A\cos(w_o t + f) \qquad \text{(Equation 2-8)}$$

The graph of these equations in Figure 2.3 shows that the displacement of the mass lags the velocity by 90° and is 180° out of phase with the acceleration.

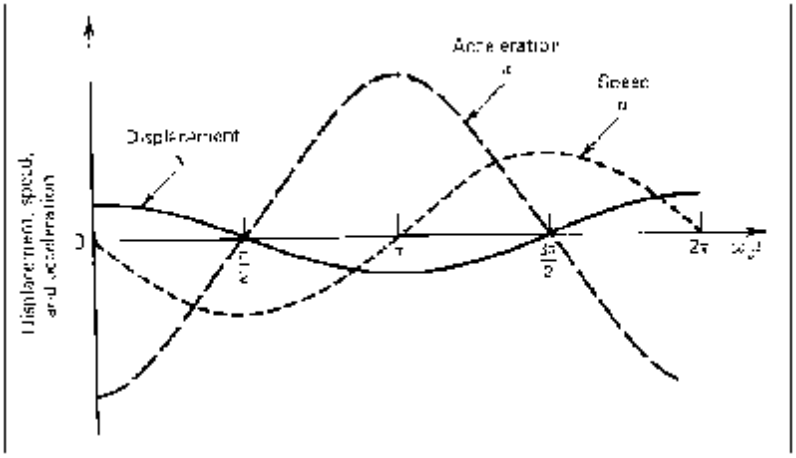

Figure 2.3: Particle displacement, speed, and acceleration of plane wave propagation [2]

2.3.2 Damped oscillation

Any real physical system has dissipative forces that act against the motion of oscillation, which cause the amplitude of oscillation to reduce with time. The type of force that causes the dissipation varies depending on the type of oscillation being examined, but all result in the overall damping of the oscillations. For the mass on a spring example examined in the last section, a viscous friction force F_r can be used to demonstrate the damping (Figure 2.4).

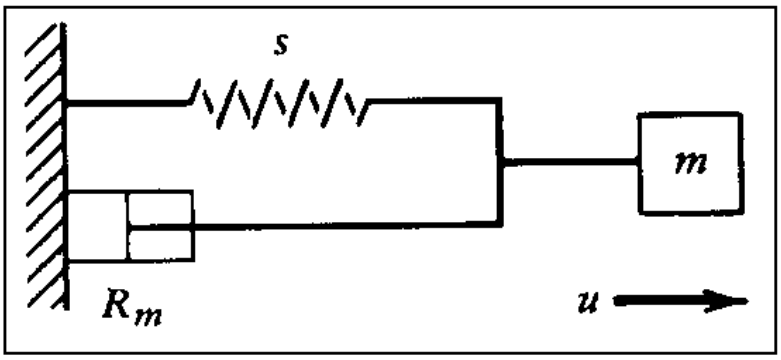

Figure 2.4: Diagram of a mass on a spring with viscous damping [2].

The force F_r is assumed to be proportional to the velocity of the mass

$$F_r = -R_m \frac{dx}{dt} \qquad \text{(Equation 2-9)}$$

where R_m is a constant representing the mechanical resistance of the system. When combined with Equation (2-4), the damped equation of oscillatory motion becomes

$$m\frac{d^2x}{dt^2} + R_m \frac{dx}{dt} + sx = 0 \qquad \text{(Equation 2-10)}$$

The completed solution to this equation is

$$x(t) = A\exp(-a_d t)\cos(w_d t + f) \qquad \text{(Equation 2-11)}$$

$$a_d = R_m / 2m \qquad \text{(Equation 2-11a)}$$

$$w_d = \sqrt{w_o^2 - a_d^2} \qquad \text{(Equation 2-11b)}$$

where a_d is the damping coefficient and w_d is the natural angular frequency of the damped oscillator. Generally, a_d is significantly smaller than w_o so that the damped natural frequency is approximately the same as the ideal natural frequency. Therefore, the

main effect of damping on oscillatory motion is an exponential decay on the amplitude of the particle motion.

2.4 Basic Wave Motion

2.4.1 The one-dimensional wave equation

The equation of motion for wave propagation can be described using the example of an ideal vibrating string. Many simplifying assumptions are made in this example in order to make the derivation easier, but the results are still very useful in developing a fundamental understanding of wave motion. If a taut string is displaced from equilibrium and then released, the displacement, shown in Figure 2.5, is seen to break into two displacements that propagate along the string in opposite directions.

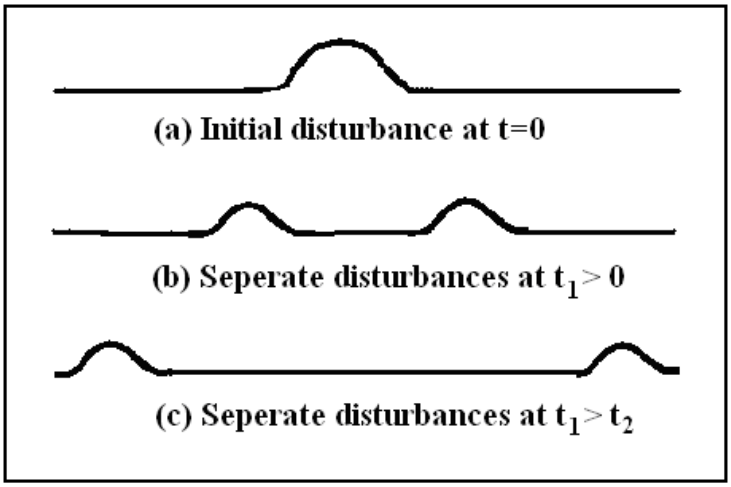

Figure 2.5: Propagation of a transverse wave disturbance along a taut string.

Also, the speed that the displacement propagates at is seen to be independent from the amplitude of the initial disturbance and instead depends only on properties of media that the wave is propagating in. For a string, the speed of propagation is given by

$$c = \sqrt{T_s / r_L} \qquad \text{(Equation 2-12)}$$

where T_s is the tension in N and r_L is the linear density of the string in kg/m. The motion of a wave propagating down a string is called a transverse traveling wave, which means that the particle displacement caused by the disturbance is perpendicular to the direction of propagation.

The equation for wave propagation is developed by considering the forces that act on the string to bring it back to equilibrium. Given a plucked string of uniform linear density and negligible stiffness, stretched to a tension T_s which is large enough so that the forces of gravity acting on the string can be ignored, the net transverse force on a small element of the string can be described by

$$df_y = T_s \frac{\partial^2 y}{\partial x^2} dx \qquad \text{(Equation 2-13)}$$

Combining this with the general equation of motion for the system,

$$df_y = r_L dx \frac{\partial^2 y}{\partial t^2} \qquad \text{(Equation 2-14)}$$

where $r_L dx$ is the mass of an element of the string, yields the one-dimensional wave equation

$$\frac{\partial^2 y}{\partial x^2} = \frac{1}{c} \frac{\partial^2 y}{\partial t^2} \qquad \text{(Equation 2-15)}$$

This differential equation has the general solution

$$y(x,t) = y_1(ct - x) + y_2(ct + x) \qquad \text{(Equation 2-16)}$$

In this solution, $y_1(ct - x)$ represents the wave traveling in the positive x direction and $y_2(ct - x)$ represents the wave that travels in the negative x direction. Possible functions for y include $\sin[w_o(t \pm x/c)]$, $\log(ct \pm x)$, and $\exp[jw_o(t \pm x/c)]$, among many others.

2.4.2 Forced vibration

Most vibrations, whether they are mechanical, electrical, or acoustical, are driven by an externally applied force. In mechanics this can be a piston, in electronics a signal generator, and in acoustics a vibrating membrane, or transducer. For a string, the simplest type of forced vibration is achieved by applying a transverse sinusoidal driving force to one end of an ideal string of infinite length.

Apply a driving force $A\cos(w_o t)$ at position $x = 0$ of an ideal string of infinite length and assume that the end of the string does not move in the x direction but is free to move in the y direction. Because the string is infinitely long, waves due to the driving force will propagate only in the positive x direction

$$y(x,t) = y_1(ct - x) \qquad \text{(Equation 2-17)}$$

Using boundary conditions and the known driving force, y_1 can be solved for as

$$y(x,t) = A\cos(w_o t - kx) \qquad \text{(Equation 2-18)}$$

where k is defined as the wave number

$$k = \frac{w_o}{c} \qquad \text{(Equation 2-19)}$$

Note that Equation (2-18) is very similar to the solution found for the differential equation of oscillatory motion, Equation (2-6). The difference here is that the phase, f, is determined by characteristics of the driving force and the media.

2.5 The Linear Acoustic Wave Equation

2.5.1 Ideal linear wave equation

As stated in Section 2.2, acoustic waves are caused by pressure fluctuations in a compressible fluid. To develop an equation for acoustic wave propagation, it is easiest to begin with the ideal case of propagation through an inviscid fluid. An inviscid fluid is a fluid in which the effects of friction due to viscosity can be ignored, meaning that the viscous effects are relatively small compared with the inertial restoring forces of the fluid [3]. It also means that losses due to attenuation through the media are ignored, making this a lossless equation for acoustic propagation. This equation is often a valid approximation because in many situations dissipation is so small that it can be ignored for the frequencies or distances of interest.

Before beginning, a few terms are defined in Table 2-1 which will aid in the understanding of the development of the wave equation. These terms are located in the List of Symbols on page viii of this thesis but are reproduced here for ease of reading.

Table 2-1 Table of useful symbols

Symbol	Unit	Description
B	Pa	Adiabatic bulk modulus
s_c	unit less	Condensation
ρ	kg/m^3	Instantaneous density
ρ_o	kg/m^3	Equilibrium density
$\vec{u}(x,t)$	m/s	Particle velocity
c_o	m/s	Speed of sound propagation
P_o	Pa	Initial pressure amplitude
ω_o	rad/s	Radial frequency
k	rad/m	Wave number
α	Np/m	Attenuation coefficient
α_κ	Np/m	Thermal attenuation
α_ν	Np/m	Viscous attenuation
η	Pa*s	Shear viscosity coefficient
η_B	Pa*s	Coefficient of bulk viscosity
κ	W/(m*K)	Thermal conductivity
c_φ	J/(kg*K)	Specific heat at constant pressure
γ	unit less	Ratio of specific heats
Z_o	Pa*s/m	Specific acoustic impedance
Ψ	m^2/s	Velocity potential
I	W/m^2	Intensity
$I(t)$	W/m^2	Instantaneous intensity
P_{RMS}	Pa	Root mean square pressure
$p(x,t)$	Pa	Acoustic pressure
T	s	Period of a wave

Using the governing physical equations for sound, the linear wave equation can be derived. These equations are the linear equation of state,

$$p \approx B * s_c \qquad \text{(Equation 2-20)}$$

the linear equation of continuity,

$$\frac{\partial r}{\partial t} + r_o \nabla \cdot \vec{u} = 0 \qquad \text{(Equation 2-21)}$$

and the linear equation of force, also known as Euler's Equation

$$r_o \frac{\partial \vec{u}}{\partial t} = -\nabla p \qquad \text{(Equation 2-22)}$$

Combining Equations (2-20), (2-21), and (2-22) yields a single differential equation with one dependant variable

$$\nabla^2 p - \frac{1}{c_o^2} \frac{\partial^2 p}{\partial t^2} = 0 \qquad \text{(Equation 2-23)}$$

This equation is the linear, lossless wave equation for the propagation of sound in fluids with phase speed c_o. Because this equation is very similar to Equation (2-15), the equation for one-dimensional wave propagation, the development of solutions already completed for Equation (2-15) can be applied here, yielding the solution

$$p(x,t) = P_o \cos(w_o t - kx) \qquad \text{(Equation 2-24)}$$

2.5.2 Lossy wave equation

Sound dissipation in a medium can be attributed to three main factors: viscous losses, heat conduction losses, and losses associated with internal molecular processes. Losses due to internal molecular processes are small compared to the other two sources of loss, and so can generally be ignored. Deriving the equation for the contribution of heat conduction losses involves a very extensive and complicated study of thermodynamics and so it is usually developed heuristically from physical arguments instead, and then simply

added to the equation for viscous losses. It is easiest to derive the lossy wave equation due only to propagation through a viscous medium and then to include losses due to thermal conduction.

All real media have some viscosity associated with them. In air, the viscosity is very low and therefore losses are small. In addition, attenuation effects in air are directly proportional to the square of the operating frequency. Therefore, in acoustic studies where the bandwidth of interest is the audible bandwidth, the frequency is low causing the attenuation to be as low as 10^{-5} Np/m. Across distances up to 1000 m, these attenuation effects are negligible and therefore attenuation due to viscous friction loss can generally be ignored, which is why the inviscid wave equation is most often used. However, attenuation increases as frequency increases, so for frequencies in the range of 30k Hz and above, the attenuation becomes as large as 10^{-1} Np/m. Even across distances as short as 1 m, the effect of this attenuation is noticeable and viscous effects must be taken into account.

To include dissipation in the form of viscosity, the governing physical equations for sound propagation must be reexamined. The equation of continuity is not changed by the presence of viscosity, and remains equivalent to Equation (2-21). The equation of state also remains the same despite the presence of viscosity because the viscous contribution to this equation is nonlinear and therefore falls out when the equation is linearized. Therefore, the equation of state remains equivalent to Equation (2-20). This leaves only Euler's Equation to be changed by the inclusion of viscosity effects.

Adding the effects of viscosity to Equation (2-22) means adding an extra term to the right side

$$r\frac{\partial \mathbf{u}}{\partial t}+\nabla p=(\tfrac{3}{4}h+h_B)\nabla(\nabla\cdot\mathbf{u})-\tfrac{1}{2}r_o\nabla^2\mathbf{u} \qquad \text{(Equation 2-25)}$$

where h is the shear viscosity coefficient and h_B is the coefficient of bulk viscosity. For a more detailed examination on the derivation of this equation and all the governing physical equations the reader is referred to Saad [4].

Combining Equations (2-20), (2-21) and (2-25) again yields a single differential equation with one dependant variable

$$\nabla^2 p-\frac{1}{c_o^2}\frac{\partial^2 p}{\partial t^2}+t_s\nabla^2\frac{\partial p}{\partial t}=0 \qquad \text{(Equation 2-26a)}$$

$$t_s=\frac{.75h+h_B}{r_o c_o^2} \qquad \text{(Equation 2-26b)}$$

This equation is the linear, dissipative wave equation for the propagation of sound in fluids. Note that it is identical to the lossless equation except for the added third term on the left hand side which can be considered the viscous dissipative term.

For a plane wave traveling in the $+x$ direction, the solution to Equation (2-26a) is defined as

$$p(x,t)=P_o\exp(-ax)\cos(w_o t-kx) \qquad \text{(Equation 2-27)}$$

where a is the attenuation coefficient in Np/m which causes the amplitude to decay in an exponential form.

Now that the differential equation and solution for lossy wave propagation have been defined, an equation for a that includes both viscous and thermal attenuation can be derived. Solving for the viscous attenuation is done by simply manipulating the above equations, yielding

$$a_v = \frac{w_o}{c_o}\frac{1}{\sqrt{2}}\sqrt{\frac{[1+(w_o t_s)^2]^{1/2}-1}{1+(w_o t_s)^2}} \qquad \text{(Equation 2-28)}$$

As mentioned above, attenuation due to thermal conduction is most easily found heuristically from physical arguments. The derivation is not done here but can be found in Blackstock [5], the equation being

$$a_k = \frac{w_o^2}{2r_o c_o^3}\frac{(g-1)k}{c_{\wp}} \qquad \text{(Equation 2-29)}$$

where g is the ratio of specific heats, k is the thermal conductivity and $c_{\wp}$ is the specific heat at constant pressure.

It can be shown that for small losses (which is the case for propagation through air, even at high frequencies), independent sources of acoustic loss can simply be summed together to create the total absorption coefficient

$$a = \sum_i a_i \qquad \text{(Equation 2-30a)}$$

$$a = \frac{w_o^2}{2r_o c_o^3}(.75h + h_B + \frac{(g-1)k}{c_{\wp}}) \qquad \text{(Equation 2-30b)}$$

The graph of Figure 2.6 shows how the total absorption coefficient increases with frequency. Note that it becomes quite significant at ultrasonic frequencies.

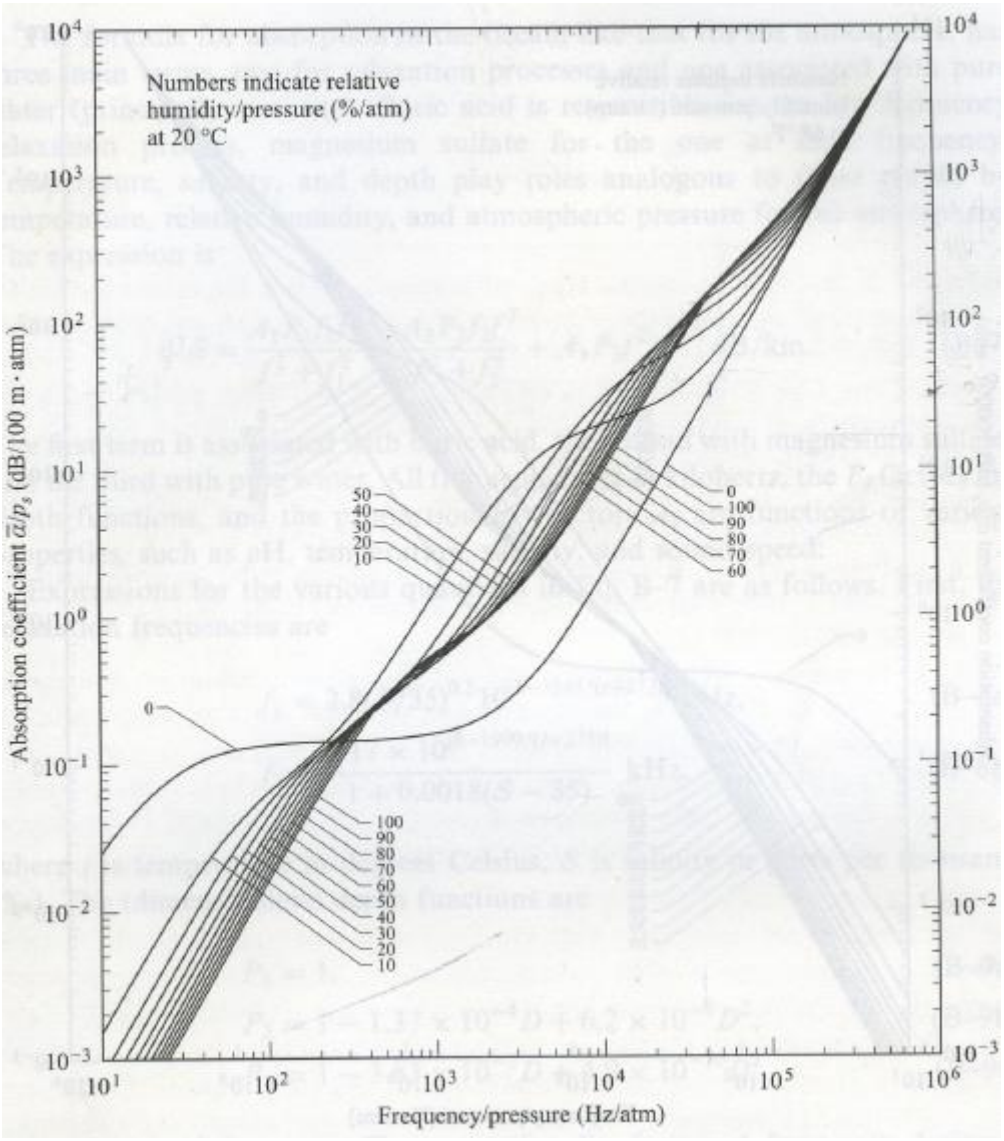

Figure 2.6: Absorption coefficient in dB/(100 m*atm) of sound in air at 20 °C and 1atm (101,325 Pa) for various relative humidities [5].

2.6 Characteristic Properties of Plane Waves

Plane waves are a special case in the study of acoustic propagation because by nature of being planar, they propagate in only one direction and, as mentioned before, have constant amplitude and phase on any plane perpendicular to the direction of propagation.

Recall also that in general, most waves can be considered planar when sufficiently far from the source, as stated in Section 2.2. Therefore defining some special properties of plane waves becomes very useful.

The solution for the pressure field $p(x,t)$ of a plane wave is described in Equation (2-24). From this, the velocity and velocity potential equations of a plane wave can easily be derived. Due to inherent properties of the plane wave already described, velocity of the wave differs from pressure by only a constant.

$$\mathbf{v}u(x,t) = \frac{\mathbf{v}p(x,t)}{r_o c_o} \qquad \text{(Equation 2-31)}$$

where $r_o c_o$ is defined as the specific acoustic impedance Z_o of the media. This impedance is analogous to the wave impedance $\sqrt{m/e}$ of a dielectric medium for electromagnetic waves and to the characteristic impedance of a Z_o of a transmission line. The velocity potential equation is almost as easily obtained, being related to pressure by a complex constant

$$\mathbf{v}\Psi(x,t) = \frac{\mathbf{v}p(x,t)}{jw_o r_o} \qquad \text{(Equation 2-32)}$$

The linear relationship between pressure and velocity is very useful, especially when developing equations for acoustic intensity. The instantaneous intensity

$$I(t) = \mathbf{v}p(x,t) * \mathbf{v}u(x,t) \qquad \text{(Equation 2-33)}$$

in W/m^2 of an acoustic wave is the instantaneous rate per unit area at which work is done by one element of the fluid medium on an adjacent element. From this, the intensity I can be defined as the time average of $I(t)$

$$I = \frac{1}{T}\int_0^T \mathbf{v}\, p(t)\mathbf{v}\, u(t)dt \qquad \text{(Equation 2-34)}$$

where T is the period of the wave. In acoustics and many other wave phenomena, the velocity of the wave particle is very hard to measure, but the pressure is a known quantity. Therefore, it is easiest to substitute Equation (2-27) into the equation for intensity, yielding

$$I = \frac{\pm P_o^2}{2 r_o c_o} \qquad \text{(Equation 2-35)}$$

It must be stressed that the $\mathbf{v}\, u(t)$ substitution is only valid when dealing with plane waves or with diverging waves that are very far from the source. If this is not the case, the intensity calculation is much more complicated.

2.6.1 Decibel scales

Sound pressures and intensities are often described using log scales because their values can vary over such a wide range; audible intensities alone can range from 10^{-12} to 10 W/m^2. Using log scales, one can define an intensity level IL of a sound intensity I by

$$IL = 10\log(\frac{I}{I_{REF}}) \qquad \text{(Equation 2-36)}$$

where I_{REF} is a reference intensity that has a value of 10^{-12} W/m^2 for air. A sound pressure level SPL of a sound pressure P_o can also be defined by

$$SPL = 20\log(\frac{P_{RMS}}{P_{REF}}) \qquad \text{(Equation 2-37)}$$

where P_{REF} is a reference pressure that has a value of 20μ Pa for air and P_{RMS} is the root mean square pressure value, defined by

$$P_{RMS} = \frac{P_o}{\sqrt{2}} \qquad \text{(Equation 2-38)}$$

Both SPL and IL have units of decibels, or dB.

2.7 The Nonlinear Wave Equation

Previously, all of the equations that were derived for acoustic propagation assumed that the propagation through air was a linear phenomenon. While this assumption is valid when explaining most small signal, low frequency acoustical phenomena, the assumption no longer holds when examining ultrasonic propagation. Nonlinear effects of both the air and the vibrating particles make significant contributions to the propagation of a sound wave through air, usually in the form of wave distortion and higher order frequency generation.

2.7.1 Nonlinear oscillation

Before deriving a nonlinear acoustic wave equation, the spring system of Section 2.3 will be revisited to see how nonlinearities can change the response of a system. Consider an undamped oscillating mass driven by a force $F(t)$. If $F(t) = A\cos(w_o t)$, it's full equation of motion can be written as

$$m\frac{\partial^2 x}{\partial t^2} + sx = A\cos(w_o t) \qquad \text{(Equation 2-39)}$$

where sx is the linear equation for the restoring force of the spring. However, if the linear restoring force is replaced with a nonlinear one,

$$sx_{NL} = sx + bx^3 \qquad \text{(Equation 2-40)}$$

then Equation (2-39) can be solved for a first and a second order approximate solution. This nonlinear situation is similar to having springs of differing "stiffness". If $b > 0$, it equates to a stiffer or harder spring, and if $b < 0$ it equates to a spring with a lower effective stiffness, or a softer spring. Solving this equation for the first and second order nonlinear approximations, one finds that the first order term is the same as the linear solution,

$$x_1(t) = A\cos(w_o t + f) \qquad \text{(Equation 2-41)}$$

and the second order approximation after many calculations and simplifications is

$$x_2(t) = A_1\cos(w_o t) + \frac{bA^3}{32mw_o^2}\cos(3w_o t) \qquad \text{(Equation 2-42)}$$

The point here is the higher order term that appears in the second order derivation and the change in amplitude of the oscillations $(A \neq A_1)$. The second term on the right hand side of the equals sign has $\cos(3w_o t)$ in it, which is defined as the third order harmonic of the original frequency, w_o. What it means is that due to the nonlinearity of the restoring force, the mass oscillation will have multiple frequency components involved rather than just the single frequency seen in the linear case.

This is a very simplified example of what one small nonlinear contribution can do to change the solution of a system. The mathematics behind the derivations for these equations was not duplicated here due to length, but can be found in Beyer [6]. The next step is to see how the inclusion of nonlinearities affects the linear acoustic wave equation.

2.7.2 The Westervelt equation

Deriving a nonlinear wave equation involves extensive mathematics and has been done in many forms and with many different contributing factors. The most complete equation that is also similar in form to the linear wave equations already derived is the Westervelt equation. This equation describes the propagation and diffraction of acoustic waves through a homogenous medium with attenuation and nonlinear behavior.

The nonlinear Westervelt equation is derived by returning again to the governing physical equations for sound propagation: the equation of state, the equation of continuity, and Euler's equation. This time, however, the equations are not linearized into their simplest form but are instead given a second order approximation based on the original full equations.

To make a second order approximation of the equation of continuity, substitute $r = r_o + r'$ into the equation, where r' is a slight deviation from equilibrium density. This substitution yields

$$\frac{\partial r'}{\partial t} + r_o \nabla \cdot \mathbf{u} = -r' \nabla \cdot \mathbf{u} - \mathbf{u} \cdot \nabla r' \qquad \text{(Equation 2-43)}$$

in which the first order terms are on the left side of the equals sign and the second order terms are on the right side. For Euler's Equation (the equation of momentum) $p = p_o + p'$, where p' is a slight deviation from equilibrium pressure, is substituted into the equation yielding

$$r_o \frac{\partial \mathbf{u}}{\partial t} + \nabla p = (\tfrac{3}{4}h + h_B)\nabla(\nabla \cdot \mathbf{u}) - \tfrac{1}{2} r_o \nabla \mathbf{u}^2 - r' \frac{\partial \mathbf{u}}{\partial t} \qquad \text{(Equation 2-44)}$$

Notice that it also contains the viscous parameters introduced in Equation (2-25). Again, the first order terms are on the left side of the equal sign and the second order terms are on the right side. The equation of state is turned into a second order approximation by expanding it in a Taylor series about the equilibrium state (r_o, s_o) and ignoring third order terms

$$p = c_o^2 r' + \frac{c_o^2}{r_o} \frac{B}{2A} r'^2 + s' (\frac{\partial p}{\partial s})_{r,0} \qquad \text{(Equation 2-45)}$$

where B/A is the parameter of nonlinearity. There are many different equations for B/A depending on the medium and what parameters are being varied. However, for ideal gases, B/A can be replaced by $(g - 1)$ [7]. Air, being composed mostly of nitrogen, can be approximated as an ideal gas giving it a B/A of 0.4.

Various manipulations of Equations (2-43), (2-44) and (2-45) and the subsequent combinations of those equations leads to a full nonlinearity equation

$$\nabla^2 p - \frac{1}{c_o^2} \frac{\partial^2 p}{\partial t^2} = -\frac{d}{c_o^4} \frac{\partial^3 p}{\partial t^3} - \frac{b}{r_o c_o^4} \frac{\partial^2 p^2}{\partial t^2} - (\nabla^2 + \frac{1}{c_o^2} \frac{\partial^2}{\partial t^2}) L \qquad \text{(Equation 2-46)}$$

where $b = 1 + B/2A$ is the coefficient of nonlinearity, d is the diffusivity of sound, and L is the second-order Lagrangian density

$$L = \tfrac{1}{2} r_o \mathbf{v}^2 - \frac{p^2}{2 r_o c_o^2} \qquad \text{(Equation 2-47)}$$

The Westervelt equation is obtained from this by discarding the term containing L, which is valid for plane waves because at first order, $p = r_o c_o \mathbf{v}$. The Westervelt equation then becomes

$$\nabla^2 p - \frac{1}{c_o^2}\frac{\partial^2 p}{\partial t^2} = -\frac{d}{c_o^4}\frac{\partial^3 p}{\partial t^3} - \frac{b}{r_o c_o^4}\frac{\partial^2 p^2}{\partial t^2} \qquad \text{(Equation 2-48)}$$

in which the first order terms are on the left side of the equal sign and the second order terms are on the right side. As mentioned before, there are many other forms of the nonlinear wave equation. However, the Westervelt equation has been found to be the most accurate for monotone directed plane progressive sound beams [8], which is what this thesis concerns itself with.

2.8 Summary

This chapter gave detailed background information on how acoustic wave propagation arises and what physical equations govern the motion. The most important items to take away from the chapter are the derivations and solutions for the ideal linear wave equation, the lossy linear wave equation, and the nonlinear Westervelt equation. All three of these will be used to characterize the longitudinal and lateral field of ultrasonic propagation, but most important is the lossy linear wave equation.

REFERENCES

[1] Möser, Michael, *Engineering Acoustics: An introduction to noise control,* New York, New York: Springer, 2004.

[2] Kinsler, Lawrence E., *Fundamentals of Acoustics*, New York, New York: Wiley Inc., 2000.

[3] Munson, Bruce, Young, Donald, and Okiishi, Theodore, *Fundamentals of Fluid Mechanics*, 4th Ed. New York, New York: Wiley Inc., 2002.

[4] Saad, Michel A., *Compressible Fluid Flow, Second Edition*, New Jersey: Prentice-Hall, Inc., 1993.

[5] Blackstock, David T, *Fundamentals of Physical Acoustics*, New York: Wiley Inc., 2000.

[6] Beyer, Robert T., *Nonlinear Acoustics*, New York, New York: Acoustical Society of America, 1997.

[7] Hamilton, Mark F. and Blackstock, David T. "On the coefficient of nonlinearity *b* in nonlinear acoustics," *Journal of the Acoustical Society of America,* vol. 83, no. 1, pp.74-77, January 1988.

[8] Huijssen, J., Bouakaz, A., Verweij, M.D., and de Jong, N. "Simulations of the nonlinear Acoustic Pressure Field without using the Parabolic Approximation," *IEEE Ultrasonics Symposium*, pp.1851-1854, 2003.

Chapter 3 Modeling of the Acoustic Signal

3.1 Introduction

Using ultrasonic interaction and reflections from an object for imaging without the use of a liquid interface between the transducer and the object being observed is a relatively new endeavor. Therefore, the research into ultrasound propagation through air is still in the first stages, looking mainly at the behavior of the transducers being used to generate the sound and the effects of air on ultrasound propagation. The majority of research that exists on ultrasound imaging in general involves propagation in water (mostly oceanic) or in biological medium because ultrasonic coupling into a liquid is much higher than it is for air and has therefore been in use longer. Because ultrasonic propagation in air is such a new field, the capabilities and deficiencies of various modeling tools are as yet unknown. This chapter first investigates some of the existing work on ultrasonic propagation in air and then details the development of this thesis, which went through many stages due to the restrictions of modeling tools.

3.2 Investigations

Up until now, the bulk of research on atmospheric acoustic propagation has focused on low frequency sound propagation and mitigation for noise pollution studies. Research into ultrasound acoustic propagation focuses on propagation in liquids such as ocean water or in biological media [1]. That is because until recently, ultrasound could not be used for imaging without using a fluid coupling media between the transducer and the item of

interest due to a large mechanical mismatch at the transducer/air interface. However, with recent developments in ultrasonic transducers, mainly in the reduction of the influence of the mechanical mismatch, it has become more feasible to use an air interface for imaging purposes.

With these advancements in ultrasound transducers have come some limited studies into ultrasound propagation in air. These studies generally examine the propagation characteristics of ultrasonic propagation but few attempt to derive fast computation models of the propagation, which would be beneficial in furthering the study of using air coupled ultrasound for imaging.

3.2.1 Study benefits and limitations

The bulk of the studies on ultrasound propagation in air have been concerned with characteristic properties of air and how they affect propagation characteristics. One such study, done by Evans, Bass, and Sutherland [2], is a detailed look at how sound attenuates in air due to various factors. Another study examines the coefficient of nonlinearity, b, for air. b is a very well characterized constant when studying oceanic or biomedical acoustic properties, but had previously not been considered important for air propagation. Studies have also been done on the beam patterns generated by ultrasonic transducers in air. One such study, performed by Benny and Hayward [3], predicts and measures the acoustic radiation generated by various types of ultrasound transducers. The authors capture some very pertinent and interesting longitudinal and lateral propagation characteristics generated

by the transducers, including 2D spread characteristics very similar in appearance to the lateral spread characteristic examined and modeled by this thesis.

What all of the previous research lacks is the generation of a fast computational method that models linear and nonlinear, longitudinal and lateral ultrasound propagation in air. One such study that is being done in this field is by Garner [4]. It furthers work done by Stoessel [5] by creating a one dimensional model that generates a single tone propagating in air. The nonlinearities inherent in air cause energy from the single tone to spread into second and third order harmonics. The effect is modeled using both a Bessel approximation and a Perturbation approximation, and is accurate to the discontinuity distance [5]

$$x_d = \frac{1}{kbM_o} \qquad \text{(Equation 3-1)}$$

where M_o is the amplitude Mach number. This model does not take into account attenuation as the wave propagates, and is only valid for longitudinal propagation.

3.3 Thesis Evolution

This thesis has evolved from a three dimensional computer model of the nonlinear propagation of a single ultrasound tone in air and its interaction at the boundary between media to a mathematical model of the linear propagation field of a single ultrasound tone in air. This change developed through many weeks of examining the limitations of available resources for modeling and by following interesting and unexpected simulation results to

their conclusions. Below is a list of the development steps, followed by a description of how one topic led to another, ending in the final thesis that this paper discusses.

- Nonlinear 3D computer model of ultrasonic acoustic wave propagation and interaction at the boundary between media.
- Nonlinear 2D computer model of ultrasonic acoustic wave propagation and interaction at the boundary between media.
- Linear 2D computer model of ultrasonic acoustic wave propagation.
- Linear mathematical model of the lateral pressure spread of an ultrasonic acoustic wave.

As discussed in Chapter 1, this thesis is part of an ongoing study into how ultrasound waves can be used to create images of and characterize items at a distance from the observer or buried under the ground.

3.3.1 Nonlinear 3D computer model

This first thesis topic was an initial foray into a hitherto unexplored area. Using COMSOL Multiphysics, a computational solver that implements finite element modeling (FEM), the possibilities of such a nonlinear 3D computer model were examined. However, it was quickly determined that COMSOL's modeling capabilities would not be able to handle this topic. According to COMSOL documentation [6], the time-dependant solver used by COMSOL can compute 3D solutions for objects of sizes approximately 5* l cubic meters. In acoustic noise studies where the frequency is low and the wavelength large, this is not a problem and therefore COMSOL is very useful. However, for ultrasound

applications where the wavelength is on the order of a millimeter, a 3D model is no longer practical (the simulation field could be no larger than a few tens of millimeters cubed). This limitation led to the revision of using a 2D model for acoustic propagation.

3.3.2 Nonlinear 2D computer model

Upon switching to a 2D model, it was found that simulations of a reasonable size (50* l rather than 5) could be completed in about an hour or two of real time for a few milliseconds of simulated time. This long simulation time sent up a red flag, pointing to the need for creating a mathematical model that would run much faster. The general idea at this point was to create the nonlinear computer model and use that along with experimental data to generate a mathematical model that would be able to compute solutions much faster than the computer model.

COMSOL Multiphysics defaults to a linear model for acoustic propagation but has a weak equation system that can be used to include nonlinearities in the model. The most common examples that COMSOL gives for incorporating nonlinearities into a model is through a nonlinear material or property. However, for acoustic wave propagation, the nonlinearities appear in the differential equation that the computer model implements to solve for the pressure of the radiating acoustic field. To incorporate this, the test function had to be used, which is a function that enables the generation of higher order derivatives and the mixing of space and time derivatives.

Before the nonlinear model could be created, a nonlinear wave equation had to be chosen. As mentioned in Chapter 2, there are many different forms of the nonlinear wave

equation in existence, and each one has its own benefits and pitfalls. The first equation that was considered was the KZK equation,

$$\frac{\partial^2 p}{\partial t \partial z} - \frac{b}{2 r_o c_o^3} \frac{\partial^2 p^2}{\partial t^2} - \frac{d}{2 c_o^3} \frac{\partial^3 p}{\partial t^3} - \frac{c_o}{2} \Delta p = 0 \qquad \text{(Equation 3-1)}$$

which has been widely used to model the paraxial region of a nonlinear sound beam. In this equation, t is the retarded time. This equation is based on a parabolic approximation, and is considered valid for directional sound beams. However, the KZK equation becomes less valid for distances close to the source and for angles 20° or more off the axis of the transducer [7]. Because this thesis examines the acoustic field at varying distances from the source and for many lateral distances, an equation that is accurate over a larger spread was desired. According to Huijssen [8], the Westervelt equation,

$$\nabla^2 p - \frac{1}{c_o^2} \frac{\partial^2 p}{\partial t^2} + \frac{d}{c_o^4} \frac{\partial^3 p}{\partial t^3} + \frac{b}{r_o c_o^4} \frac{\partial^2 p^2}{\partial t^2} = 0 \qquad \text{(Equation 3-2)}$$

which is a full nonlinear wave equation, is a much more comprehensive equation that accurately depicts the acoustic field both near and far from the source and at higher degrees from the beam axis. In fact, the KZK equation can be considered an approximation of the Westervelt equation. An explanation and derivation of the Westervelt equation can be found in Section 2.7.2.

For the implementation of the Westervelt equation in COMSOL, Dr. M.A. Zikry, a professor of Mechanical and Aeronautical Engineering at North Carolina State University, was consulted for his extensive knowledge in finite element modeling. The Westervelt equation is a fourth order partial differential equation. For a fourth order differential

equation, the shape used to create the element mesh of the model should have 8 nodes (see Figure 3.1) for best resolution of the nonlinear effects. The default mesh size in COMSOL is a 3 node triangle mesh, and the highest mesh that can be utilized is a 4 node mesh. This limitation raised some initial concerns with COMSOL's ability to accurately model the nonlinear equation.

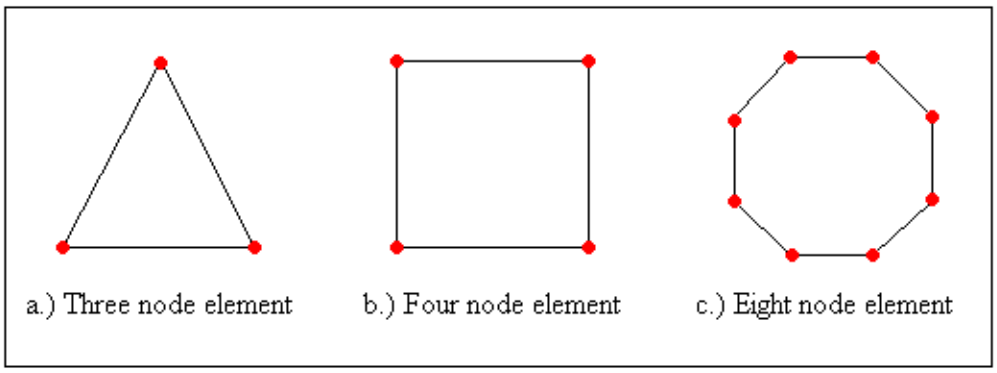

Figure 3.1: Various mesh shapes for finite element modeling. Computations are performed at the nodes, where different elements meet. Higher order computations require higher noded mesh elements.

The model was meshed using the four node shape.

The next step was to put the Westervelt equation into a form the COMSOL solver could use. As mentioned before, COMSOL has a weak form for representing nonlinear equations in which the test function is used to define derivatives above 2nd order and mixed space and time derivatives. The test function is not described here but more information can be found in the book Finite Element Method by Reddy [9], or any other introductory finite element book. As an example of the test function, COMSOL defines the linear wave equation using the weak form as

Weak term: $-px*test(px)-py*test(py)$ (Equation 3-3a)

Time-dependant weak term: $\frac{ptt*test(p)}{c_o^2}$ (Equation 3-3b)

where px, ptt, etc. are the first and second derivatives of pressure with respect to x and t, respectively. Converting the Westervelt equation using the test function yields an equation of

Weak term: $-px*test(px)-py*test(py)$ (Equation 3-4a)

Time-dependant weak term: (Equation 3-4b)

$$\frac{1}{c_o^2}ptt*test(p)-\frac{d}{c_o^4}ptt*test(pt)-\frac{b}{r_o c_o^4}Psqtt*test(Psq)$$

Note the Psq term. This term comes from the $\frac{\partial^2 p^2}{\partial t^2}$ term of the original equation, and Psq is defined elsewhere in the model to be the square of pressure. However, the solver can not access any dependent variables other than p; it does not recognize Psq as a dependent variable. It quickly became apparent that the test function COMSOL utilizes would not be able to handle the higher orders of the nonlinear Westervelt equation. It was therefore decided that it would be much more time efficient to switch to a linear simulation model and heuristically incorporate nonlinearities later.

3.3.3 Linear propagation model

The next and final revision to the thesis topic was to do linear propagation models in place of nonlinear propagation models. The linear wave equation, which COMSOL implements by default, was used along with a 3 node mesh. Alongside the computer

model, physical experiments were run in an anechoic chamber for comparison. Using results from both of these, mathematical models were created that depict the longitudinal and lateral propagation of ultrasonic waves in air. The method and results of the thesis are described in more detail in Chapters 4 and 5.

3.4 Summary

Most examinations to date have studied ultrasound imaging through a liquid interface. Now that transducers are being made that can couple a useful amount of energy into the air, it is necessary to gain a strong understanding of ultrasound propagation in air. There is currently very little information available on linear and nonlinear propagation in air. The goal of this thesis is to develop a model that will determine how a wave of given amplitude and frequency will propagate through the atmosphere. This thesis accomplishes that goal by combining experimental results and computer modeling to generate a mathematical representation of the two dimensional propagation of the ultrasound wave.

REFERENCES

[1] Cristini, C., Piraux, J., and Sessarego, J. P., "Experimental Benchmarks for Numerical Propagation Models: Comparison Between Numerical Results and Tank Experiments for Deep and Shallow Water Environments," in *Theoretical and Computational Acoustics, 1997*, Edited by Teng, Y.C., Singapore: World Scientific Publishing Co., 1999, pp. 667-677.

[2] Evans, L. B., Bass, H. E., and Sutherland, L. C. "Atmospheric Absorption of Sound: Theoretical Predictions", *The Journal of the Acoustical Society of America,* vol. 51,no. 5, pp. 1565-1575, September 1972.

[3] Benny, G., Hayward, G., and Chapman, R. "Beam Profile Measurements and Simulations for Ultrasonic Transducers Operating in Air", *The Journal of the Acoustical Society of America,* vol. 107, no. 4, pp.2089-2100, April 2000.

[4] Garner, Glenwood III, MatLab code general_fr.m and Perturbation_3rd_Harmonic.m, received November 25, 2007.

[5] Stoessel, Rainer, "Air-Coupled Ultrasound Inspection as a New Non-Destructive Testing Tool for Quality Assurance", Ph.D. Dissertation , University of Stuttgart, February 2004

[6] COMSOL Multiphysics Modeling Guide, *The Weak Form,* COMSOL Multiphysics, 2006.

[7] Averkiou, M.A. and Hamilton, M.F. "Nonlinear distortion of short pulses radiated by plane and focused circular pistons", *The Journal of the Acoustical Society of America*, vol. 102, no. 5, pp.2539-2548, 1997.

[8] Huijssen, J., Bouakaz, A., Verweij, M.D. and de Jong, N. "Simulations of the Nonlinear Acoustic Pressure Field without using the Parabolic Approximation", *IEEE Ultrasonics Symposium*, pp.1851-1854, 2003.

[9] Reddy, J. N, *Finite Element Method*, 3rd ed. New York: McGraw-Hill, 2006.

Chapter 4 Simulation Models

4.1 Introduction

In this chapter, the models that will be used in the empirical development of the mathematical model are presented. An anechoic chamber used for physical experiments is described, along with a computer model that will be used to confirm the experimental data. The longitudinal propagation characteristics extracted from both the anechoic chamber and the computer model are compared to expected results in order to verify the accuracy of both.

4.2 Method

In acoustic studies, longitudinal propagation of plane waves through a medium is a well understood phenomenon. How an acoustic wave spreads laterally is less understood and not mathematically characterized. Therefore, one can confirm the accuracy of models and experiments using known longitudinal characteristics. Once proven, the models can be used as a basis for new contributions to the field. For this thesis, the main steps were as follows:

1. Develop an experimental model using an anechoic chamber with a 40k Hz transducer for signal generation.
2. Generate a computer model of the anechoic chamber using COMSOL Multiphysics.

3. Using known characteristics and mathematical models of longitudinal wave propagation, determine the accuracy of both the physical experiments in the anechoic chamber and the simulation results of the computer model.
4. Capture the lateral propagation characteristic of the transducer signal in the anechoic chamber.
5. Confirm the measured lateral propagation data of the anechoic chamber using results from the computer model.
6. Develop mathematical models of the lateral propagation characteristic using MatLab and Excel.

Steps one through three, the creation and verification of the simulation models, will be discussed in this chapter. Steps four through six, the extraction and characterization of the lateral propagation, will be discussed in Chapter 5.

4.3 Development of the Models

4.3.1 Anechoic chamber

The anechoic chamber is a box with exterior dimensions of approximately 3.65m long, 2.44m wide, and 1.82m tall. It has been raised off the floor by 0.1 m in order to reduce vibration interference being transferred into the chamber through the building floor. Due to the thickness of the absorbent materials used in the chamber, the internal dimensions are approximately 3.04m long, 1.93m wide, and 1.32m tall. The attenuation panels that line the floor, walls and ceiling of the chamber are all comprised of the same materials, the layering of which can be seen in Figure 4.1.

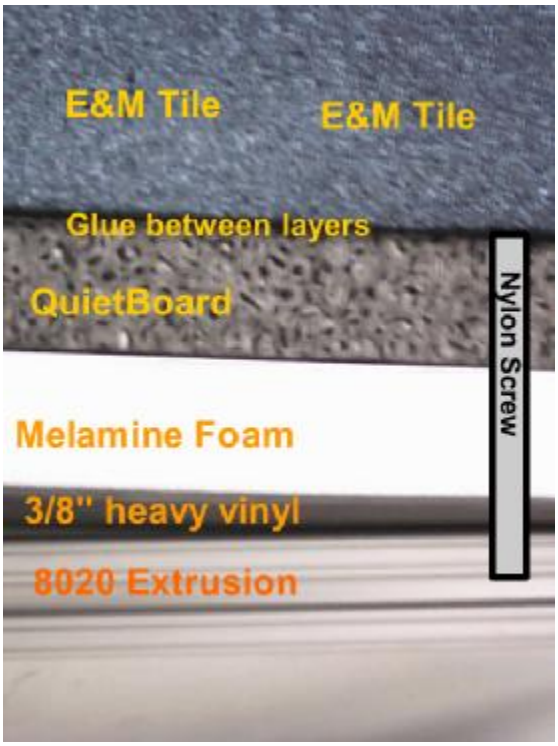

Figure 4.1: The makeup of the acoustical blocking material on the anechoic chamber walls, floor, and ceiling.

The first layer is Acoustiblok sound isolation membrane of 3.0mm thickness. It is a high-density vinyl material that provides almost two-thirds of the through-wall attenuation above 1 kHz [1]. At every seam and joint in the Acoustiblok layer, Acoustical Sound Sealant Caulk and Acoustiblok Iron Grip Tape was used to further improve the soundproofing. Layered on top of the Acoustiblok were 0.61 m by 1.21 m panels of 25.4 mm thick Melamine Foam, a lightweight, open-cell material, glued to 25.4mm thick Quiet Board™, a foam material comprised of porous expanded polypropylene beads, and then one layer of E&M Tile, a foam material comprised of cone shapes for RF absorption, shown in Figure 4.2.

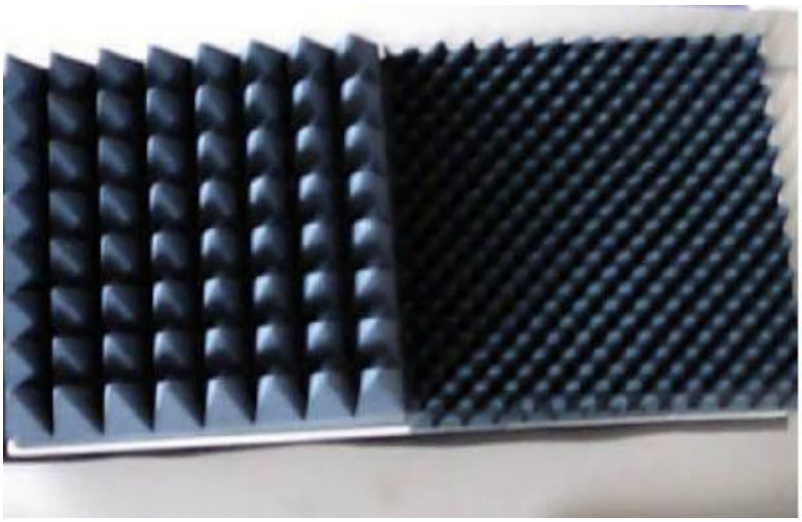

Figure 4.2: E&M Tile used for the outermost layer in the chamber absorption tiles.

The various layers were glued together using the Acoustical Sealant. These layers caused the walls of the chamber to attenuate both transmitted and reflected acoustic energy, giving total attenuation of up to 100 dB insertion loss and 45 dB return loss [2].

The chamber experiment was setup with a single 40k Hz transducer with 2 Pa initial pressure amplitude placed at one end. The transducer was a 5.715 cm AIRMAR AT 51 Air Transducer and development board that emits a focused sound beam which propagates as a plane wave. The beam axis of the transducer was found and marked out in the chamber using fishing line, an acoustically invisible material. A microphone was then placed at intervals along the beam axis to record pressure levels. The microphone used to record data was a PCB Piezotronic condenser microphone connected to a PXI-5922 high-speed digitizer. A schematic of the experimental setup is depicted in Figure 4.3.

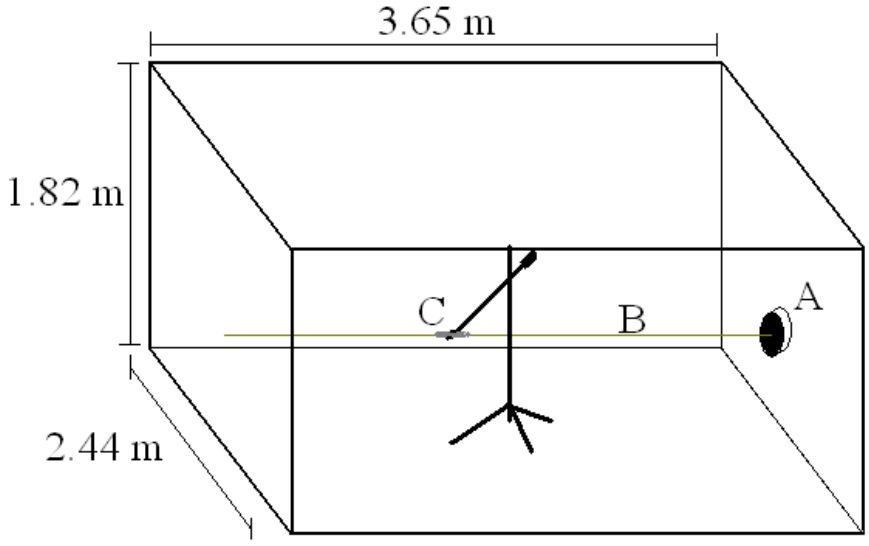

Figure 4.3: Schematic of the anechoic chamber setup for wave propagation experiment.
A: 40k Hz Transducer
B: Line along beam axis
C: Microphone

The microphone began recording peak pressure values at 0.1778 m from the source and continued recording values at varying intervals for a total distance of 2.0955 m. The separation distance of the anechoic chamber was 0.47 m.

4.3.2 Computer model

A 2D linear idealized finite element model (FEM) of the anechoic chamber was generated using COMSOL Multiphysics. For a full report on the generation and simulation of the model, see Appendix A. The model consists of a rectangular chamber that contains a transducer which generates a 40k Hz sound wave. Due to limitations of the time-dependent solver used by COMSOL, the size of the chamber and transducer had to be scaled down considerably.

COMSOL uses a variable-order, adaptive BDF method to solve transient problems. When this method is applied to wave equations, it can introduce significant numerical damping of high frequencies if the time step is too long. This condition yields a limiting step size related by the CFL number [3].

$$CFL = \frac{c_o t_{\max}}{h} \qquad \text{(Equation 4-1)}$$

The CFL number is a dimensionless number that represents the fraction of an element that the wave travels in one time step. For the problem being simulated, convergence with respect to the time step is reached as long as CFL < 0.04. In the above equation, c_o is the speed of sound in the medium, $t_{\max}$ is the limiting step size, and h is the maximum mesh element size chosen by

$$f_o = \frac{c_o}{hN} \qquad \text{(Equation 4-2)}$$

where N is the number of elements per wavelength required to resolve a harmonic wave with accuracy [4] and f_o is the source frequency. Setting N to 5 (a sufficient number for a wave of 40k Hz) yields an h value of 1.715mm. Using this in the CFL equation and setting CFL to 0.025, the maximum time step for proper simulation is 125ns. Given these mesh and time step limitations and in order to maintain a reasonable simulation time, the chamber area had to be kept smaller than approximately 42 cm x 42 cm.

Knowing that the total chamber size had to fit within the above dimensional constraints, a one-tenth scale model of the chamber was initially implemented. This reduction led to a 2D computer model of the chamber with dimensions of 0.365 m long by

0.244 m wide. Applying the same reduction to the transducer leads to a transducer width of 5.715 mm. However, the wavelength of the signal at 40k Hz is 8.575 mm. In order to ensure that the computer model transducer behaves similar to the physical transducer in the anechoic chamber, its dimensions would need to be wider than a wavelength. The transducer was therefore rescaled to a value of 1.13276* l , a number chosen randomly so that it would be neither an exact multiple nor a pi fraction of lambda. Even with these size limitations, the computer ran out of memory before the simulation could be computed. Therefore, the model was further reduced to a size of 0.21 m long by 0.1342 m wide, a reduction by a factor of approximately 1.8.

The final FEM solved for 40,908 elements with 82,256 total degrees of freedom, which took approximately one hour of real time for 1.5 ms of simulation time. From this, one can clearly see the inadequacy of an FEM solution for a quick calculation of wave interactions. See Appendix A-6.2 for a full report on the mesh generation. The final chamber computer model is shown in Figure 4.4.

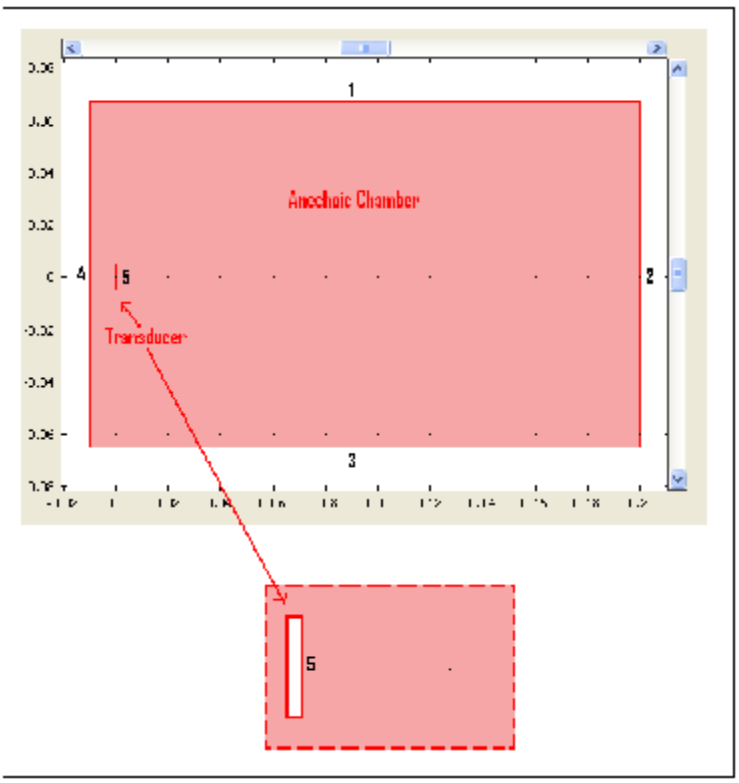

Figure 4.4: COMSOL computer model of the Anechoic Chamber. The chamber has been scaled down to 21 cm by 13.42 cm, with a 9.7 mm transducer. A close up of the transducer is shown in the bottom of the figure

To model the high acoustic absorption of the walls of the chamber, the boundaries of the subdomain (boundaries 1, 2, 3, and 4 in Figure 4.1) were given a radiation condition with zero initial pressure, which yields no wave reflections back into the chamber. The area within the chamber was given the characteristics of air, which corresponds to a density of 1.2 kg/m^3 and a sound speed of 343 m/s. See Appendix A-6.3.4 for a detailed report on the boundary definitions and Appendix A-6.3.5 for the subdomain definitions.

The transducer was placed at vertical center on the left hand side of the chamber so that longitudinal wave propagation would be in the +x direction. The vibrating membrane of the transducer was represented by line 5 in Figure 4.4. The boundary condition for line 5 was set as a monotone pressure source with a signal of $P_o \sin(w_o * t)$, producing a single frequency wave that propagates in the x direction. See Appendix A-6.1.1 for a detailed report on the source definition. P_o was set to 2 Pa and w_o was set to 2*pi*40k Hz, which is the same initial pressure and frequency output by the transducer that was used in the physical experiments. Because the source is an ideal straight line, it will exhibit propagation characteristics of a line source rather than a circular transducer. This means that the wave will propagate as a cylindrical wave rather than a plane wave, creating a propagation variation between the computer model and the anechoic chamber. The effects of this propagation variation will be explained in detail in Section 4.4.

4.4 Verification of the Models

To verify the accuracy of both the anechoic chamber and the computer model, the longitudinal propagation response of each was compared to known results reported in literature. The expected result for a plane wave propagating in the far field is exponential peak decay along the beam axis. This result can be used to verify the validity of the anechoic chamber because the transducer generates a focused beam that propagates as a plane wave in the far field. However, as mentioned in Section 4.3.2, the computer model is not exact in its physical representation of the transducer; the transducer was modeled using

a line source, which should display more lateral dispersion due to cylindrical spreading than the physical transducer in the anechoic chamber.

4.4.1 Expected results

The expected result for the anechoic chamber was exponential peak decay along the beam axis due to the attenuation effects of air, described by Equation (2-27) and in detail in Section 2.5.2. The attenuation coefficient a can be calculated exactly using Equation (2-30b), but a reasonable approximation can be found by examining the graph of Figure 2.6. Assuming a room pressure of 1 atm and a relative humidity of 40% [5], the attenuation coefficient at 40k Hz, according to the graph, is 1.7 dB/m. It can be converted to a pressure attenuation coefficient by the equation

$$\overline{a} = 8.686 * a \qquad \text{(Equation 4-3)}$$

where $\overline{a}$ is the attenuation coefficient in dB/m and a is the attenuation coefficient in Np/m [6]. Doing so yields an expected attenuation coefficient of 0.196 Np/m.

MatLab was used to plot the expected peak decay function

$$p(x) = 2\exp(-0.196x) \qquad \text{(Equation 4-4)}$$

which is shown in Figure 4.5. This graph can be considered the expected results against which the measured characteristic of the anechoic chamber will be compared.

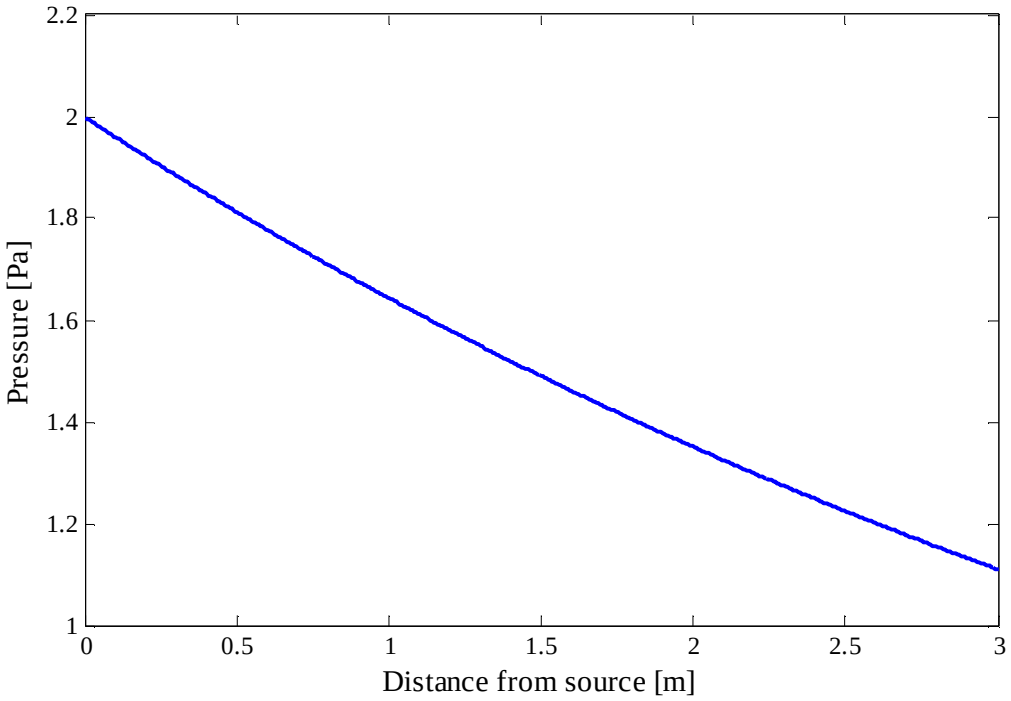

Figure 4.5: Graph of the expected exponential longitudinal peak decay for the measured anechoic chamber results.

In the computer model, the transducer is modeled by a straight line source. In the far field, a straight line source exhibits some cylindrical spreading as well as attenuation, and so it decays by a rate of $1/\sqrt{x}$ along with the exponential decay described above [6]. MatLab was used to plot the expected peak decay of the computer model

$$p(x) = \frac{2}{a\sqrt{x}} \exp(-0.196x) \qquad \text{(Equation 4-5)}$$

which is plotted in Figure 4.6. This graph can be considered the expected results against which the validity of the computer model will be compared.

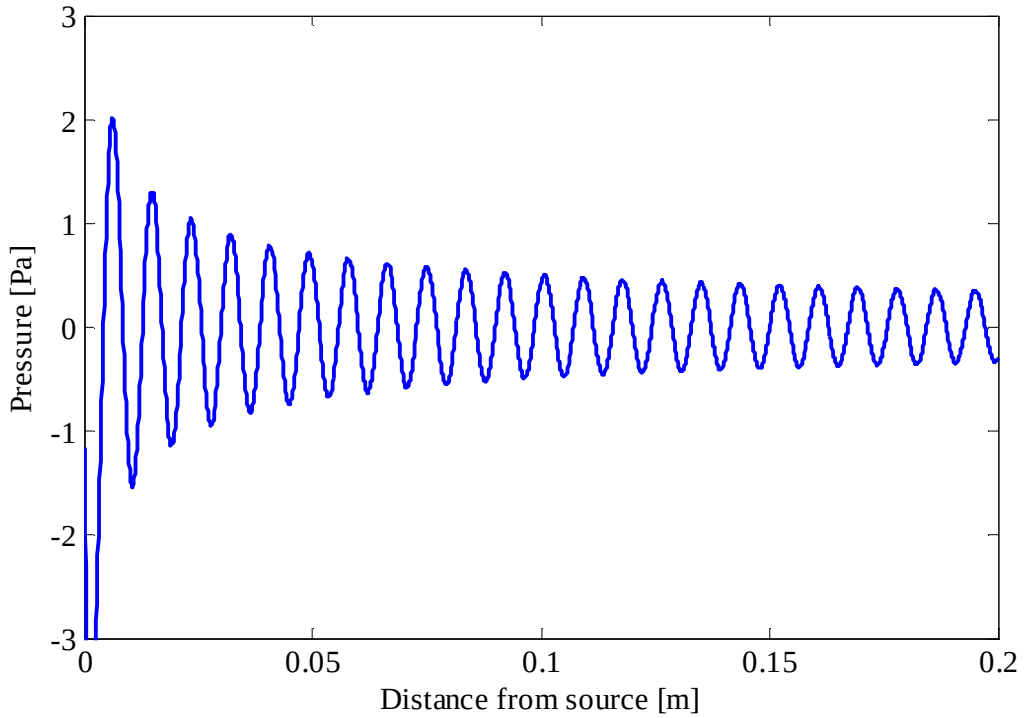

Figure 4.6: Graph of the expected longitudinal peak decay for the computer model results.

The coefficient "a" in Equation (4-5) is a linear scaling factor included to ensure that the equation follows the physical response of the system. Without that scaling factor, the pressure at any distances less than 1 m would be larger than the initial pressure amplitude. As this is physically impossible, the scaling factor needs to be included to ensure that the equation represents what actually occurs during wave propagation.

4.4.2 Anechoic chamber verification

Once the chamber was set up and ready for experiments, data was captured in the manner discussed in Section 4.3.1. The instrumentation used to record the data was a

LabView program written by Garner and Skeen [7] that displayed the information as both a time domain and frequency domain result, in both Pa and dB. The data was recorded for continuous time, but had to be stopped each time the microphone was repositioned. This resulted in the data being captured in discrete packets at intervals along the beam axis. The data therefore needed to be recombined in order to compare it to the expected results of Figure 4.5. A sample of the raw data collected from the chamber is shown in Figure 4.7a, while the final combination of peak decay data along the beam axis is shown in Figure 4.7b.

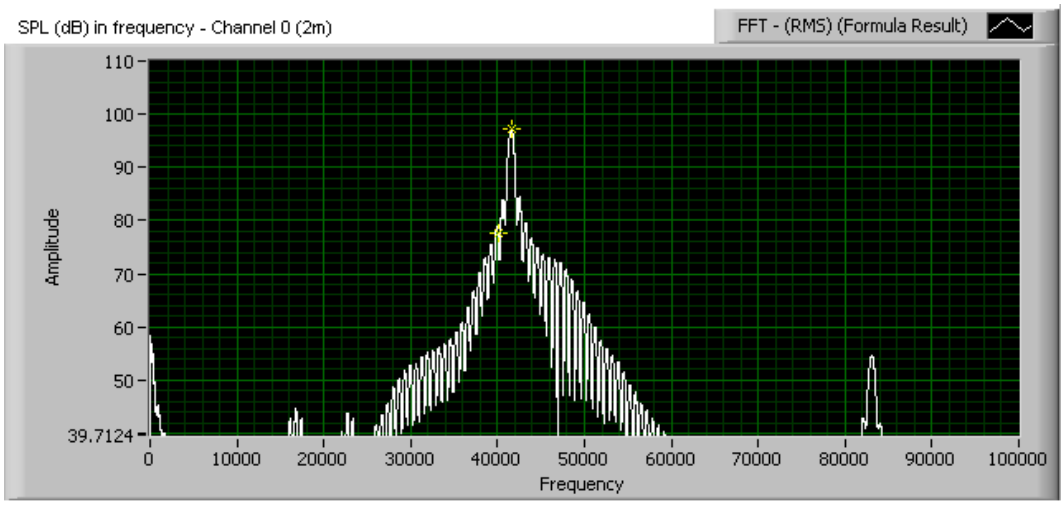

Figure 4.7a: Raw data packet collected from measurements in the anechoic chamber. This data represents the peak RMS pressure value in dB at 0.19m from the transducer. Data was collected in discrete packets, then combined to create the graph in Figure 4.7b.

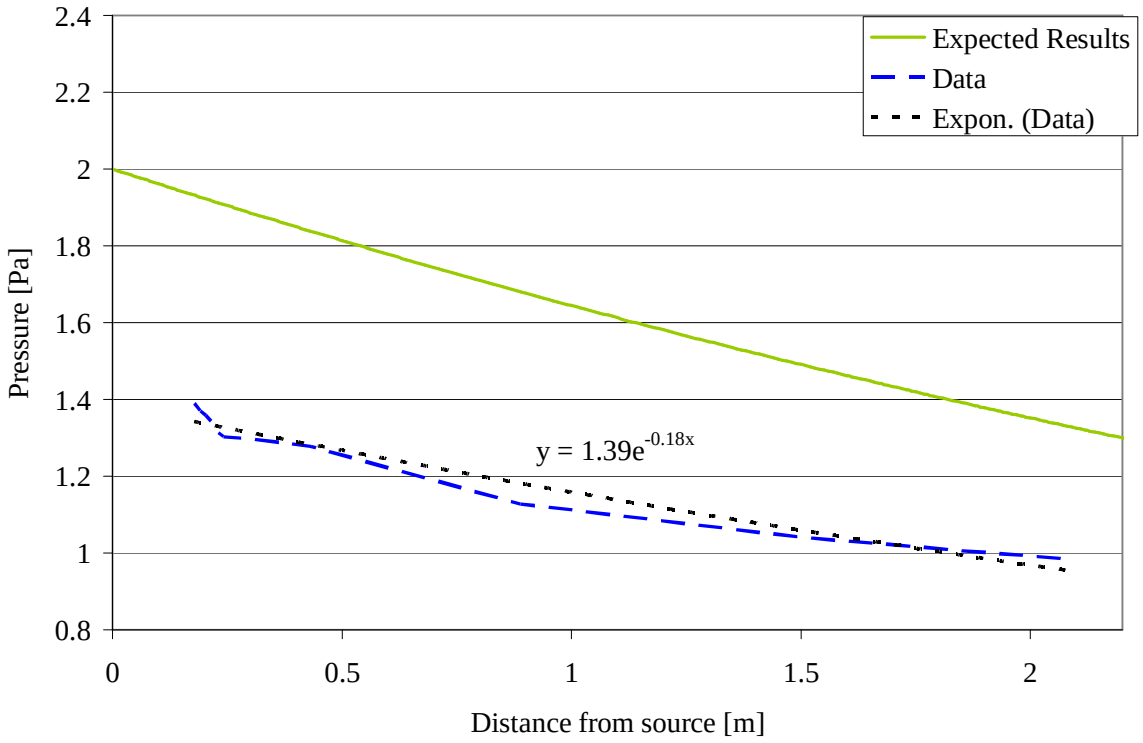

Figure 4.7b: Measured longitudinal peak pressure decay along the beam axis taken from the anechoic chamber (blue data line) with an exponential equation fit (black data line and equation). The expected decay results are also plotted for comparison (green data line).

A copy of the raw chamber data captured for longitudinal peak decay can also be found in Appendix B-1.

An exponential curve fit was performed on the peak decay results from the anechoic chamber in order to determine the experimental attenuation coefficient. The result of this curve fit was the equation

$$p(x) = 1.39\exp(-0.18x) \qquad \text{(Equation 4-6)}$$

which shows an attenuation factor of 0.18 Np/m, very close to the expected value of 0.196 Np/m. The initial pressure value, 1.39 Pa, is very low assuming that the transducer actually emits a 2 Pa initial amplitude. The difference is a result of near-field differences in decay.

The wave amplitude does not decay in the same exponential form in the near field, but rather actually decays much faster. What is important in determining accuracy is that the attenuation coefficients in the far field are close. Therefore, of concern in the graph is the rate at which the expected and experimental results decay as opposed to their actual position in the y direction.

The closeness of the two attenuation coefficients confirms that the anechoic chamber setup and method for gathering data are fairly accurate. The error between the two numbers can be attributed to the fact that the pressure within the chamber is not exactly 1atm nor is the relative humidity exactly 40%. Relative humidity of a climate controlled room can vary from 20% - 60% [5], causing a to vary from 0.09 Np/m to 0.2 Np/m. Some error can also be attributed to slight microphone misplacements from the beam axis when gathering the data, although this kind of error was minimized by varying placement distances and by repeating measurements.

4.4.3 Computer model verification

The longitudinal propagation characteristic of the computer model, shown in Figure 4.8, was extracted from the simulation results by plotting the pressure along the beam axis line that extends from $x = 0$ to $x = 0.2$ m, $y = 0$ m in the computer model of Figure 4.4.

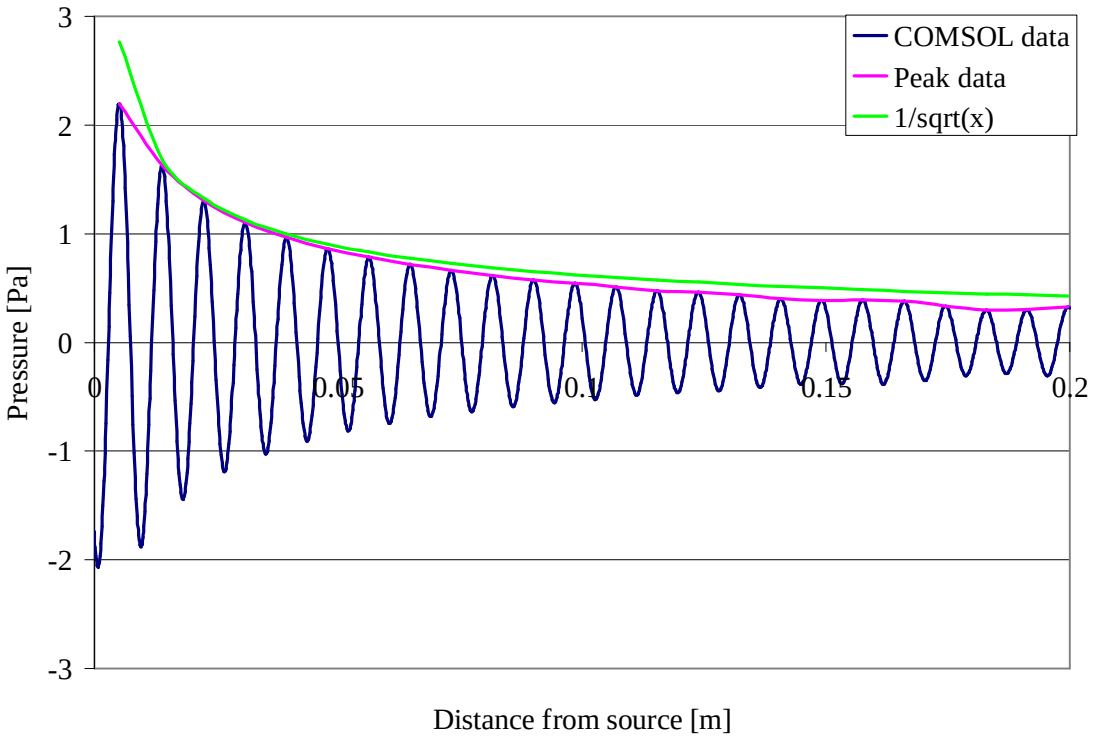

Figure 4.8: COMSOL computer model results for the longitudinal peak pressure decay along the beam axis (blue data line). The peak pressure values of the computer results were recorded and plotted (pink data line) for better comparison with the expected results (green data line).

The expected results were superimposed on the COMSOL results in order to better interpret the accuracy of the model. Comparing the peak decay of the COMSOL results with the expected cylindrical spreading plus exponential decay, it is apparent that COMSOL gives a very accurate response. The peak amplitudes decay at a rate inversely proportional to the square root of distance from the source. The computer model is therefore verified to be accurate.

4.5 Summary

An experimental model was created using an anechoic chamber with a 40k Hz, 2 Pa transducer and microphone. A computer model of the anechoic chamber was also created that mirrored the components of the anechoic chamber. The two models were verified for accuracy using expected longitudinal decay characteristics; exponential peak decay in the anechoic chamber and cylindrical spreading along with exponential peak decay in the computer model. The results of the computer model vary from those of the anechoic chamber because the transducer in the computer model is represented using a straight line source while the actual physical transducer is a circular piston. A straight line source is expected to exhibit some cylindrical spreading, but a circular piston that generates a focused beam is expected to propagate as a plane wave. Because of this, the results of the computer model are expected to vary from those of the anechoic chamber.

REFERENCES

[1] Stoessel, Rainer, “Air-Coupled Ultrasound Inspection as a New Non-Destructive Testing Tool for Quality Assurance”, Ph.D. Dissertation , University of Stuttgart, February 2004

[2] Garner III, G., Wilkerson, J. and Skeen, M. *“Acoustic-RF Anechoic Chamber Construction and Evaluation,”* North Carolina State University, 2007

[3] Courant, R., Friedrichs, K.O., and Lewy, H. “On the partial difference equations of mathematical physics," *IBM Journal*, vol. 11, pp.215-234, 1956.

[4] COMSOL Multiphysics Acoustics Module, *Transient Gaussian Explosion,* COMSOL Multiphysics, 2006.

[5] Minnesota BLUE FLAME GAS Association: 'Humidity and the Indoor Environment' http://www.blueflame.org/datasheets/humidity.html

[6] Blackstock, David T, *Fundamentals of Physical Acoustics*, New York: Wiley Inc., 2000.

[7] Skeen, M. and Garner, Glenwood III. Labview program Monitoring_Tone_Generation.vi, 2007.

Chapter 5 Development of the Mathematical Model

5.1 Introduction

Once the model and anechoic chamber were confirmed to be accurate, the lateral propagation characteristic along a constant phase arc was examined from both the anechoic chamber and the computer model and a mathematical model was developed that describes both longitudinal and lateral ultrasonic propagation. Because of the differences between the anechoic chamber and the computer model discussed in Chapter 4 (the transducer in the computer model is represented using a line source which exhibits some cylindrical spreading, as opposed to the plane wave propagation of the focused circular piston in the anechoic chamber), it is expected that the lateral propagation characteristic of the computer model will spread out further than the lateral propagation characteristic from the focused transducer of the anechoic chamber.

5.2 Lateral Propagation Characteristic

5.2.1 Lateral Propagation in the anechoic chamber

The lateral propagation of the acoustic wave is defined in this paper to be the pressure distribution along an arc of constant phase perpendicular to the longitudinal beam axis. The pressure wave generated by the transducer in the anechoic chamber travels forward as a plane wave. Therefore, the constant phase arc of the propagating wave is a line perpendicular to the direction of propagation. Lateral propagation data was obtained in the anechoic chamber by recording pressure values along a line perpendicular to the

longitudinal beam axis. Data was gathered from the chamber at two distances from the source: first at 1.524 meters from the source and then at 0.899 m from the source. Lateral data was collected in increments varying from 0.635 cm to 1.27 cm along a line perpendicular to the beam axis. The increments were varied to give better accuracy in measuring and to reduce error. Again, because the data had to be captured in discrete packets at intervals along the lateral spread line, it needed to be recombined. The lateral propagation data taken from the chamber is shown in Figure 5.1. A copy of the raw chamber data captured for lateral propagation can also be found in Appendix B-2.

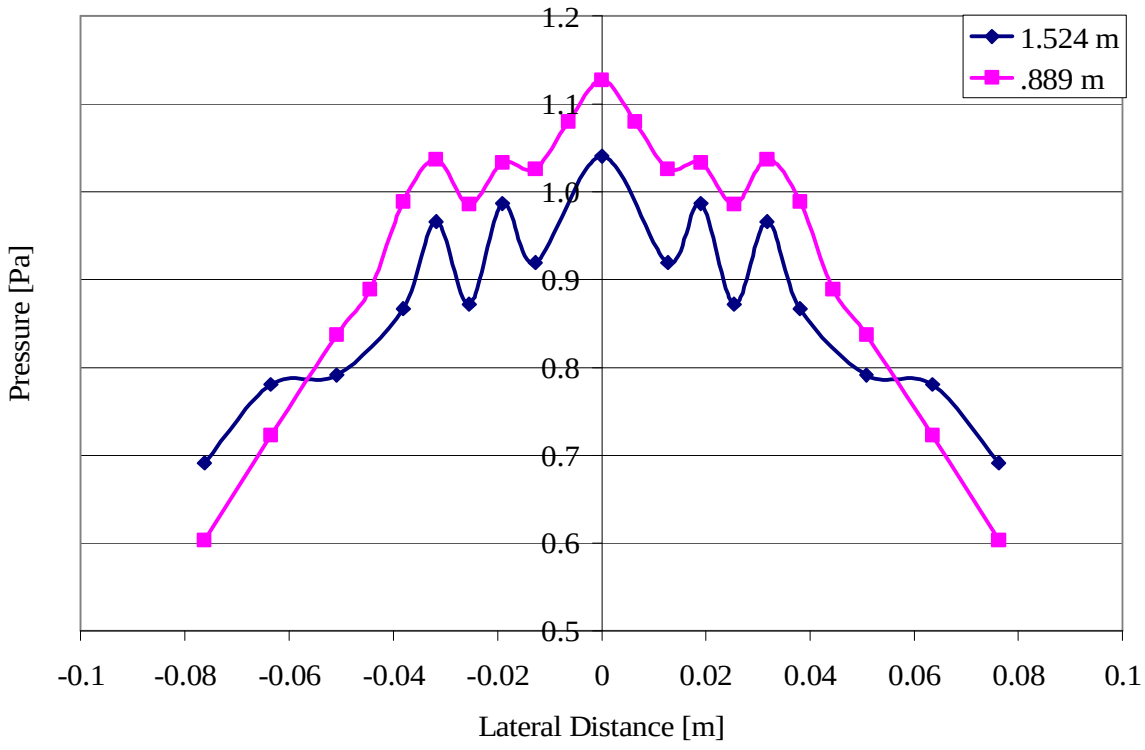

Figure 5.1: Measured lateral propagation characteristic from experiments in the anechoic chamber. Data was recorded at 0.889 m from the source (pink data line) and 1.524 m from the source (blue data line).

The data shows that the pressure drops off as you move laterally away from the beam axis. It also shows that the lateral pressure characteristic takes on a sinusoidal shape that becomes more pronounced as the wave moves away from the source. Also, the average pressure distribution in the lateral direction evens out as the wave moves away from the source. Note that at a certain lateral distance, the sinusoidal variation appears to stop and the lateral pressure simply drops off in a Gaussian or parabolic form. This is because the transducer emits a focused beam; outside the area of that beam the pressure will simply drop off to equilibrium because there is no forward propagation and therefore no lateral pressure characteristic.

It can be concluded that energy from the acoustic wave is moving laterally as well as longitudinally as the wave propagates. The lateral movement takes on a sinusoidal characteristic shape, with the average lateral pressure becoming more constant as the wave moves further away from the source.

5.2.2 Lateral propagation in the computer model

The measured lateral propagation characteristic observed in the anechoic chamber was confirmed by comparison with the lateral propagation characteristic of the computer model. A transient simulation was run for 1.5 ms and the lateral propagation characteristic was then extracted from the simulation results for comparison. The full 2D results of this simulation are displayed below in Figure 5.2.

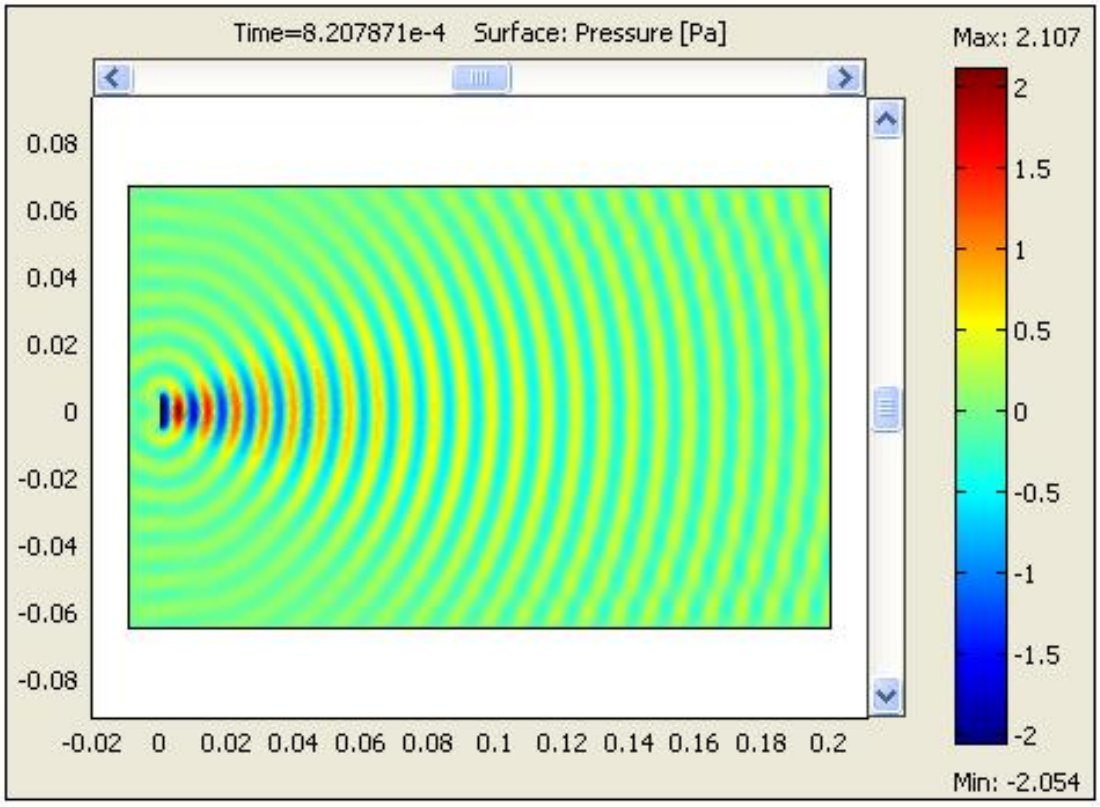

Figure 5.2: Transient 2D computer simulation results of a 40k Hz sound wave propagating through an anechoic chamber from a line source transducer. The scale on the right is expressed in Pascals, while the x and y axes are in meters.

Because the transducer in the computer model exhibited some cylindrical spreading, finding the constant phase arcs was not as straightforward as it was in the anechoic chamber. The constant phase arcs were found for varying distances from the source (Figure 5.3) by following the 0 degree phase point of the wave at time t in the $\pm y$ direction.

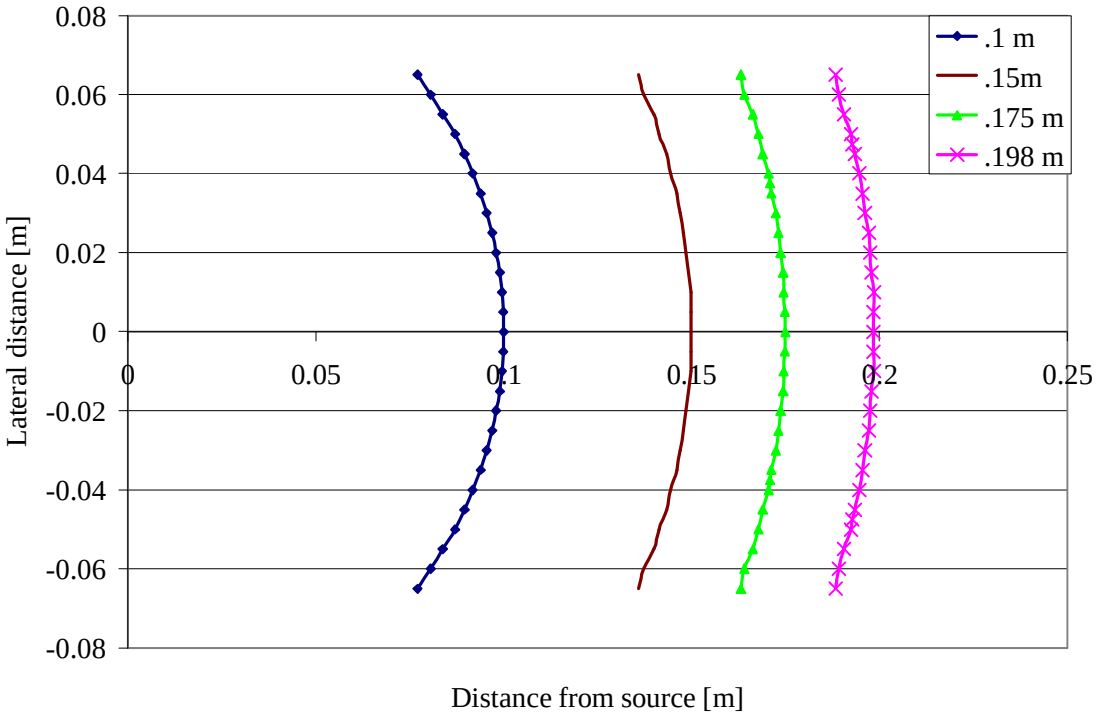

Figure 5.3: COMSOL computer model constant phase arcs of sinusoidal propagation at varying distances from the source. Note that as the arc gets further from the source it approaches a straight line, or plane wave appearance.

The constant phase arcs of the computer model are slightly curved due to the cylindrical spreading caused by the use of a line source to model the transducer. Note that as the constant phase arc gets further from the source, it looks more like a plane wave response. The lateral spread characteristic of the acoustic propagation can be extracted from the COMSOL computer model results by recording the pressure values along the constant phase arcs. Doing so yields the waveforms of Figure 5.4.

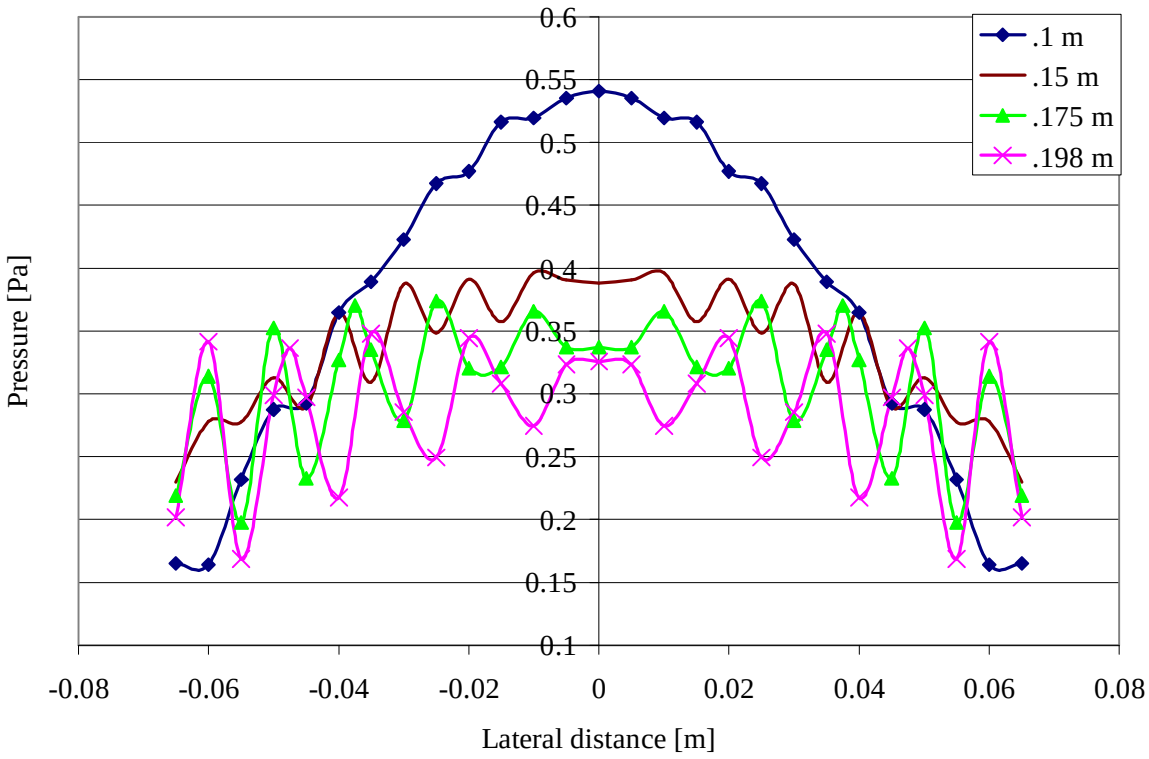

Figure 5.4: COMSOL computer model lateral pressure characteristic, data was extracted by plotting pressure values along the constant phase arcs of Figure 5.3.

The computer model results show a very similar characteristic as those of the anechoic chamber. The lateral sinusoidal variation is present and increases as the wave moves away from the source, and the lateral sinusoidal amplitude increases as the signal moves away from the beam axis. An effect that is more noticeable here than in the measured results is that as the lateral sinusoid approaches the edges of the sound beam, the lateral sinusoidal amplitude begins to decay, most apparent in the 0.15 m pressure characteristic. The average pressure along the constant phase arc becomes more constant as

the wave moves away from the source; this effect is more dramatic in the computer results due to the high curvature of the constant phase arcs close to the source.

The main difference between the anechoic chamber and the computer model is that the computer model lateral propagation characteristic extends further into the lateral direction than does the measured anechoic chamber results. This was an expected result, and can be explained by the difference in transducer representations. Other slight differences between the model and the anechoic chamber results can be attributed to the fact that the computer model is ideal and does not take into account nonlinearities or variations in density and air temperature. Gee and Sparrow [1] found that nonlinearities are the primary cause of disagreement between measured and linearly predicted acoustic behavior at high frequencies. There is also a factor of error introduced because the measurements in the chamber had to be taken in individual packets and then combined, while the computer model can calculate the instantaneous pressure at all points in the chamber at the same time.

It can be concluded that energy from the acoustic wave is moving laterally as well as longitudinally as the wave propagates. The lateral movement takes on a sinusoidal characteristic shape, with the average pressure becoming more constant as the wave moves further away from the source. This characteristic shape is further confirmed by running simulations at varying frequencies and amplitudes: all simulations show the characteristic lateral propagation recorded above, although they vary as to lateral frequency of oscillation and distance from the source at which the oscillations become apparent. Shown below is an

example of the further computer tests that were run; it is a 50k Hz acoustic wave with an initial pressure of 894 Pa and it also displays the characteristic lateral propagation.

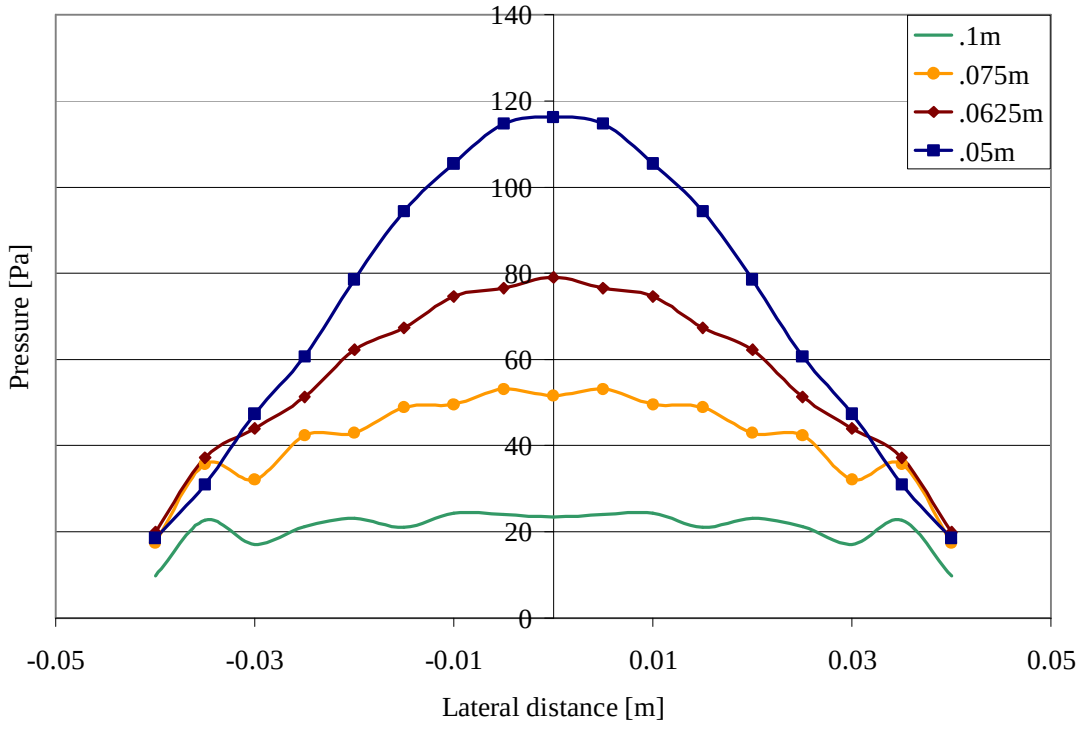

Figure 5.5: COMSOL computer model lateral pressure characteristic of a 50k Hz acoustic wave with 894 Pa initial pressure amplitude.

The characteristic sinusoidal variation of the lateral propagation is present in both the experimental model and the computer model, and is therefore confirmed as a naturally occurring phenomenon. This is a previously unnoted phenomenon that can be characterized using mathematical models which will help expedite future studies of acoustic interaction between two separate waves or even between waves and objects.

5.3 Mathematical Model

The results from the computer model were used to generate the mathematical models because the computer model yielded a full two dimensional field of data points to work with. Using the measured results from the anechoic chamber would have been less practical because of the dearth of data points available. Once the mathematical models are developed, they will be used to generate the measured results in the chamber to show that they accurately depict the propagation characteristics of a physical transducer.

5.3.1 Polynomial Fit

Due to the sinusoidal nature of the lateral spread, the waveform was initially fit with a polynomial function

$$p(x,y,t) = a\cos(by) * (\sum_{m=1}^{4} A_m y^m + 1) + \sum_{n=0}^{6} B_n y^n + \frac{P_o}{d\sqrt{x}} \exp(-ax)\sin(w_o t - kx)$$

(Equation 5-1)

which yielded a good fit to the lateral propagation, as displayed in Figure 5.6.

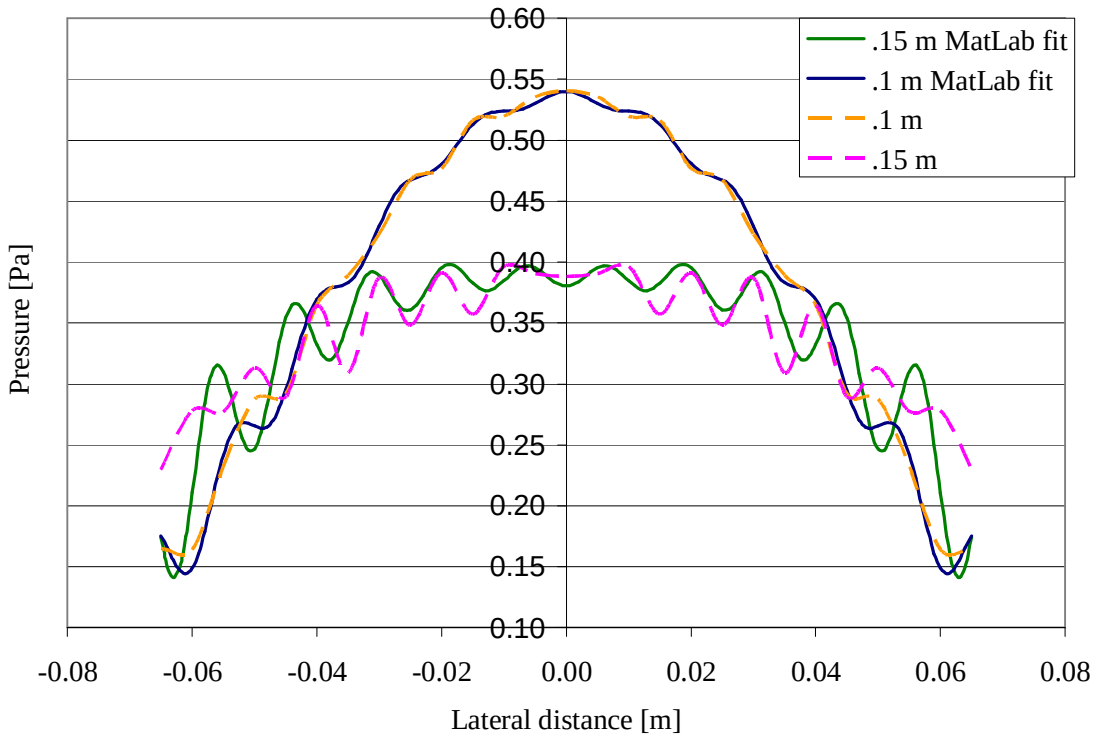

Figure 5.6: Polynomial curve fit to the computer model lateral propagation characteristic.

The constants in Equation (5-1) rely on axial and lateral distances as well as physical properties of the medium. The values of the polynomial coefficients for these curve fits are displayed in Table 5-1. The first term in the summation generates the sinusoidal variations along the constant phase arc, the second term is a polynomial that generates the main pressure arc, and the third term sets the $y(0)$ point of the pressure curve.

Table 5-1 Coefficient values for Equation (5-1)

	.1 m	.15 m
a	0.004	-0.008
b	2π*75	2π*80
A_1	-0.1	-0.1
A_2	2000	2000
A_3	50	50
A_4	100	100
B_0	0.536	0.388
B_1	4E-10	5E-9
B_2	-121.83	-4.85
B_3	2E-6	8E-7
B_4	2907.6	-1.8E4
B_5	3E-5	4E-5
B_6	1E41	2E41
P_o	2	2
α	0.2	0.2
d	12.9	12.9

The fit compares very well with the computer model results; it shows the sinusoidal variation of the lateral propagation increasing with distance from the source, as well as the increase in sinusoidal amplitude as the signal moves away from the beam axis. What this equation does not capture is the damping of the sinusoidal amplitude as the lateral distance approaches the edge of the sound beam. While the polynomial gives a good fit, a lower order equation that can capture the decrease of sinusoidal amplitude at the beam edges as well as all the other lateral propagation characteristics would be more beneficial.

5.3.2 Hermite-Gaussian fit

It is interesting to note that a Hermite-Gaussian (HG) function can also be used to generate a mathematical model for the lateral pressure spread. In order to do so, a program was first written in MatLab to generate and plot the HG functions. The full MatLab code for this and other MatLab programs is shown in Appendix C. The HG function [2] is defined by

$$HG_n(y) = (-1)^n * H_n(y) * \exp(\frac{-y^2}{2}) \qquad \text{(Equation 5-2)}$$

where $H_n(y)$ is the Hermite polynomial

$$H_n(y) = (-1)^n * \exp(\frac{y^2}{2}) * \frac{d^n}{dy^n}[\exp(\frac{-y^2}{2})] \qquad \text{(Equation 5-3)}$$

These equations yield curves of the characteristic shapes displayed in Figure 5.7.

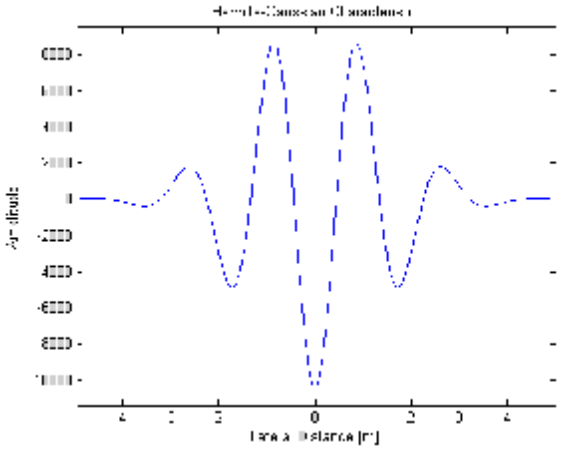

Figure 5.7a: 12th order HG function

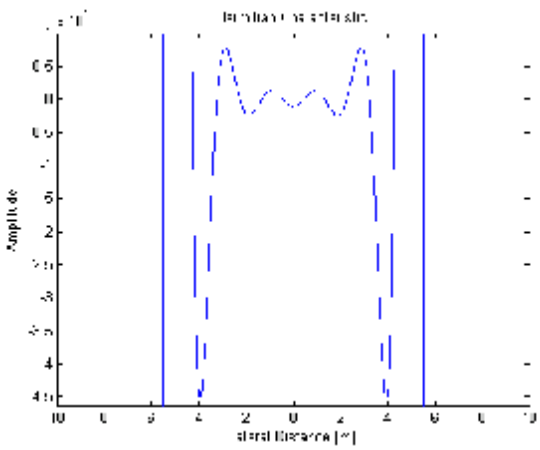

Figure 5.7b: 12th order Hermite polynomial. Higher orders increase the amplitude and generate more oscillations

As the order of the HG function increases, the number of oscillations the wave form generates before settling out increases. The amplitude of the oscillations also increases, by powers of ten, as the order of the function is increased. Therefore, the order used to capture the longitudinal spread characteristic will vary depending on the lateral distance that is being examined. The wider the distance, the higher the order of the HG function will have to be, because a wider lateral spread will mean more lateral oscillations captured.

A possible curve fit for the lateral pressure spread characteristic can be generated using a low ordered HG function with a sinusoidal function

$$p(x, y, t) = \frac{y}{a}\sin(\frac{y}{b}) + HG_n(y) \qquad \text{(Equation 5-4)}$$

which is displayed in Figure 5.8. However, this is again just a sinusoidal fit that uses the HG function rather than a polynomial function, as seen in Equation (5-1), to generate the main pressure arc.

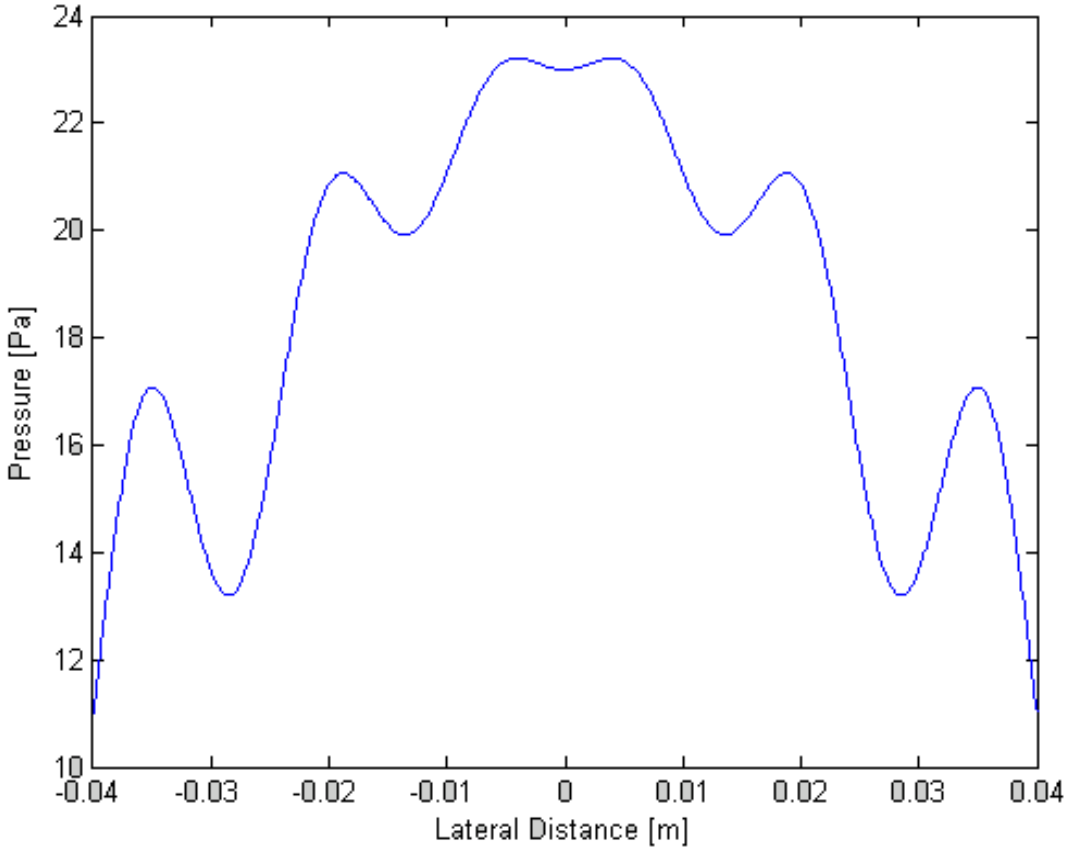

Figure 5.8: Graph of Equation (5-4). A close fit to the lateral propagation characteristic, but it is still basically a sinusoidal fit, rather that a Hermite-Gaussian fit.

Ideally, the HG function itself would be used alone to generate the full lateral pressure characteristic.

The Hermite-Gaussian equation for the lateral pressure propagation characteristic was developed in an empirical manner. The HG curve amplitudes had to be first reduced by many orders of magnitude in order to make them usable. They were then fit to the lateral propagation characteristic using curve fitting tools. The final equation for the Hermite-Gaussian fit was

$$p(x,y,t) = [A * H_{20}(\frac{y}{a}) \exp(\frac{-(y/b)^2}{2}) * \sum_{n=0}^{2} B_n y^n * \cos(\frac{w_o}{d} t - \frac{k}{d} x - e) + F * HG_6(\frac{y}{f}) + .1] * \frac{P_o}{g\sqrt{x}} \exp(-ax) * \sin(w_o t - kx)$$

(Equation 5-6)

where the values of the constants are determined by lateral and longitudinal distances as well as physical properties of the media. The values of the coefficients for Equation 5-6 are displayed in Table 5-2.

Table 5-2 Coefficient values for Equation (5-6)

	.1 m	.15 m
A	1E-9	1E-9
a	0.009	0.0084
b	0.0126	0.009
B_0	0.005	0.02
B_1	0	0
B_2	25	740
d	3.99	3.99
e	3.92E4	3.92E4
F	0.06	0.06
f	.04	.075
g	12.9	12.9
α	.2	.2

The first Hermite-Gaussian function sets the sinusoidal variation of the lateral propagation. It is multiplied by a polynomial function for scaling purposes and then by a cosine function, which sets the lateral movement of the sinusoidal variation. The order of

the first HG function determines the number of oscillations that will occur in the lateral direction. The second HG function creates the main lateral pressure arc on which the sinusoidal variation sits. The graph of this equation is shown in Figure 5.9.

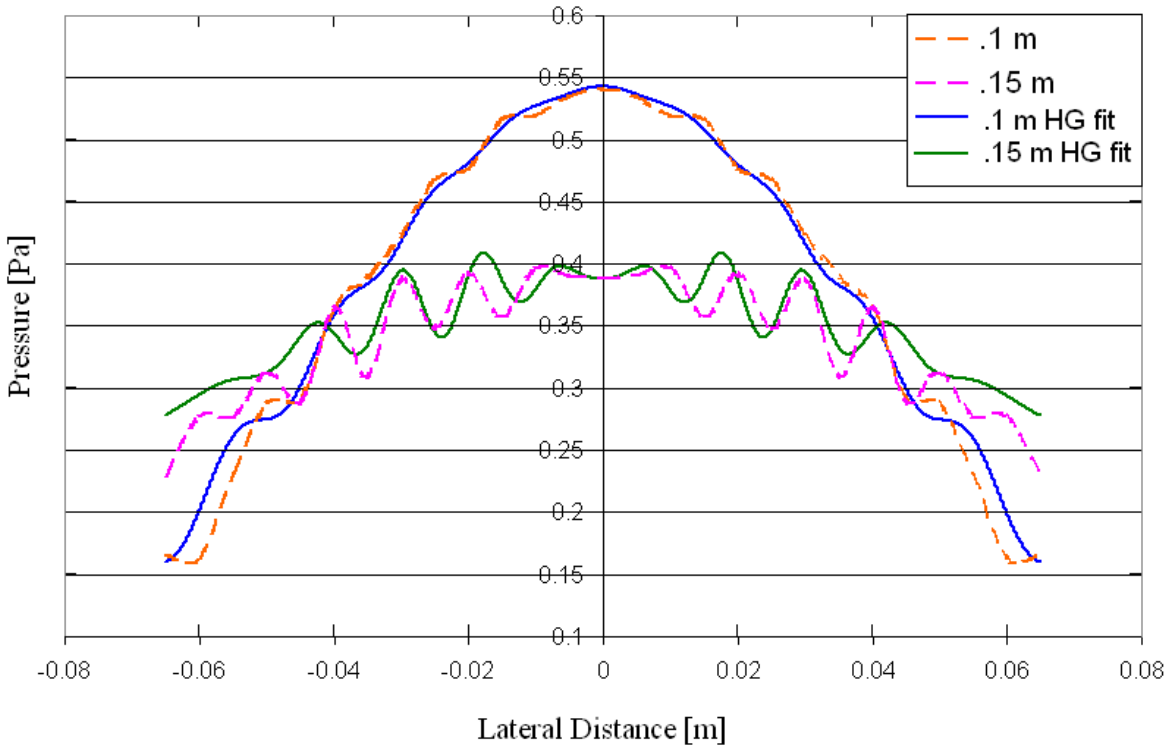

Figure 5.9: Hermite-Gaussian curve fit to the computer model lateral propagation characteristic.

The Hermite-Gaussian fit matches the lateral propagation characteristic very well. It shows all the lateral propagation characteristics that the sinusoidal fit displayed, and also captures the sudden decay of the lateral sinusoid amplitude at the sound beam edge. It can be concluded that the HG fit is a valid model of the lateral pressure spread. To further confirm this, Equation (5-6) was also fit to the measured results from the chamber, shown in Figure 5.10.

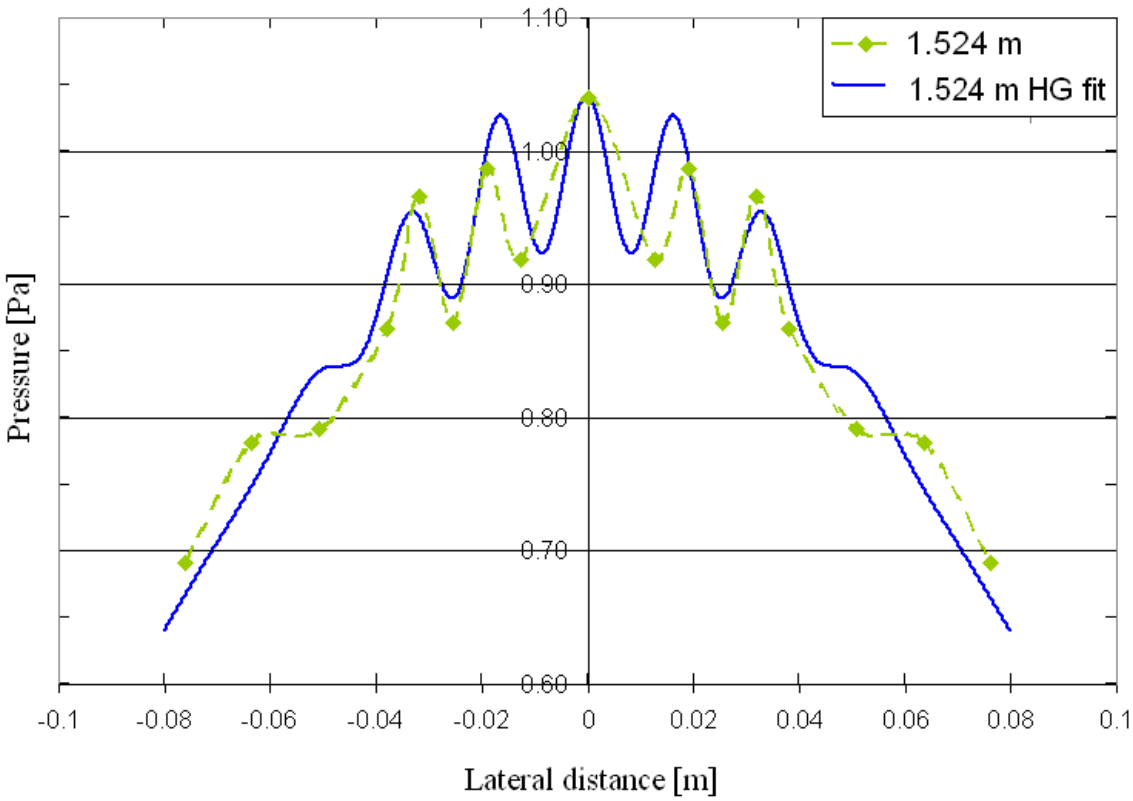

Figure 5.10: Hermite-Gaussian curve fit to the measured lateral propagation characteristic.

The Hermite-Gaussian fit is better than the polynomial fit when describing the propagation characteristic because it has fewer constants to define than does the polynomial fit, as well as being a more accurate representation. Using fewer constants leads to a simpler model definition and therefore a simpler relationship between material properties and propagation properties.

5.4 Summary

This chapter presents a linear mathematical model of the longitudinal and lateral propagation of single tone ultrasound acoustic waves through air. In order to create the mathematical model, lateral propagation characteristics along an arc of constant phase were first extracted from both the anechoic chamber and the computer model. Differences between the two can be attributed to the nonlinear affects of the chamber not being modeled in the computer, as well as the fact that the computer model representation of the transducer did not match the physical transducer. However, they displayed a similar characteristic shape which was fit with mathematical equations. The most important of the equations is the Hermite-Gaussian fit that was generated because it utilizes fewer coefficients and has a more accurate match of the characteristic.

REFERENCES

[1] Gee, K. L., and Sparrow, V. W. "Measurement and Prediction of Nonlinearity in Outdoor Propagation of Periodic Signals," *The Journal of the Acoustical Society of America*, vol. 120, no. 5, pp.2491-2499, November 2006.

[2] Abramowitz, M. and Stegun, I. *Handbook of Mathematical Functions*, New York, New York: Dover, 1972

Chapter 6 Conclusion

6.1 Conclusions

A mathematical model that predicts the lateral and longitudinal propagation of an ultrasonic acoustic wave in the atmosphere has been developed. It was designed using both experimental results recorded in an anechoic chamber and a linear propagation finite element model. The longitudinal propagation results from these models were used along with expected results from literature to confirm the accuracy of the anechoic chamber and the computer model. Lateral propagation characteristics were then extracted from the measured chamber data and confirmed using the computer model. The results from the computer model were fit with polynomial and Hermite-Gaussian functions to create mathematical models. The Hermite-Gaussian function gave a more accurate fit than the polynomial and utilizes fewer constants which means a simpler relationship between material properties and propagation characteristics.

It was also determined that using a finite element solver to model nonlinear ultrasound propagation in air is not a feasible endeavor. It was also determined that, due to the small wavelength of the signals, three dimensional linear computer models would be too small to be useful in any applicable propagation simulations. It was shown that two dimensional linear finite element models are possible on the order of up to fifty wavelengths, but that simulation time to compute such a large model is on the order of one hour of real time for approximately one millisecond of simulation time, making a computer model impractical for fast computation models of ultrasound propagation in air.

6.2 Future Work

The next step in developing a propagation model for ultrasound in the atmosphere is to combine nonlinear effects into the linear mathematical model. It needs to be determined whether nonlinearities in the air contribute to the lateral propagation as well as the longitudinal propagation. It is my belief that nonlinearities won't play as big a role in the lateral propagation as they do in longitudinal propagation because the frequency with which the amplitude oscillates in the lateral direction is much slower than that of the longitudinal. Once the nonlinear effects are incorporated, the coefficients of the mathematical model need to be characterized using physical properties of the wave and the propagation media. Once that is done, the mathematical model will be complete, requiring only frequency and amplitude input to determine the nonlinear propagation characteristic at any distance from the source.

APPENDIX

Appendix A: COMSOL model report

This model report was generated by COMSOL. It is a record of the development and simulation steps of the computer model generated for this thesis.

COMSOL Model Report

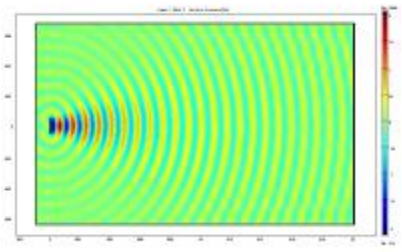

1. Table of Contents

2. Model Properties

Property	Value
Model name	40kHzLinearWave
Author	JoAnna Vetreno
Company	NC State

Department	ECE
Reference	
URL	
Saved date	Nov 14, 2007 4:07:40 PM
Creation date	Aug 28, 2007 9:18:46 AM
COMSOL version	COMSOL 3.3.0.405

File name: C:\COMSOL33\JoAnnaPractice\2PaConstPhase40k.mph

Application modes and modules used in this model:

- Geom1 (2D)
  - Pressure Acoustics (Acoustics Module), transient analysis

3. Constants

The constants used in the model to describe subdomain, source, boundary, and simulation properties. They are entered directly into the Options>Constants field.

Name	Expression	Value	Description
c_air	sqrt(gamma*Pamb/rho_air)		speed of sound in air
rho_air	Pamb*M/(R*T)		density of air
h_max	c_air/(f0*N)		mesh size
N	5		
f0	40000[Hz]		source frequency
t0	1/f0		
CFL	.025		
t_step	CFL*h_max/c_air		simulation time step
w0	2*pi*f0		source frequency
A	rho_air*c_air^2		
tdel	t0*6		for pulse source
tdur	t0*3		for pulse source
beta	1+.5*BoA		2nd order coefficient of

			nonlinearity
Pamb	101325[Pa]		ambient density
k	n*R*T/(V*Pamb^2)		
Po	2[Pa]		source amplitude
M	.029[kg/mol]		molecular weight
R	8.314472[J/(K*mol)]		univ. gas constant
T	293.15[K]		temperature
Vrms	sqrt(3*R*T/M)		
Vbar	sqrt(8*R*T/(pi*M))		
Vp	sqrt(2*R*T/M)		
gamma	1.4		ratio of specific heat
b	.016		VanDerWaal's correction
squig	M/(b*rho_air)		
J	(2*(2*squig-3)^2)/(3*(squig-1)*(6-5*squig))		
V	1[m/s]		
n	42		
alpha	n*R/(V*Pamb)		
theta	sqrt(3*M/(R*T*k*rho_air+9))		
dcdp	(1-gamma^-1)*c_air*k/(2*T*alpha)+J/(2*rho_air*c_air)		
BoA	2*rho_air*c_air*dcdp		
B	BoA*A		
CoA	3*B^2/(2*A^2)-(c_air^2*k*rho_air-1)^2/(2*T^2*alpha^2)-(2*theta^2*(3+2*theta))/(3*(theta-3)^2)		
C	CoA*A		
Gair	pi/(2*rho_air^2*c_air^5)		
Fair	6*pi/c_air		
eta	1+.5*CoA		3rd order coefficient of nonlinearity
Pr	.7		

vis	1.78e-5[kg/(m*s)]		thermal viscosity
v	vis/rho_air		kinematic viscosity
mus	.6		ub/u for air
delta	v*(4/3+mus+(gamma-1)/Pr)		diffusivity of sound
k0	w0/c_air		
lam	c_air/f0		
tw	lam*1.13276		

4. Global Expressions

The equations used to define the source function. They are entered into the Options>Expressions>Global Expressions field

Name	Expression	Description
wave	Po*sin(w0*t)	

5. Geometry

The anechoic chamber model. This section displays the points, boundaries, and subdomains that make up the model.

Number of geometries: 1

5.1. Geom1

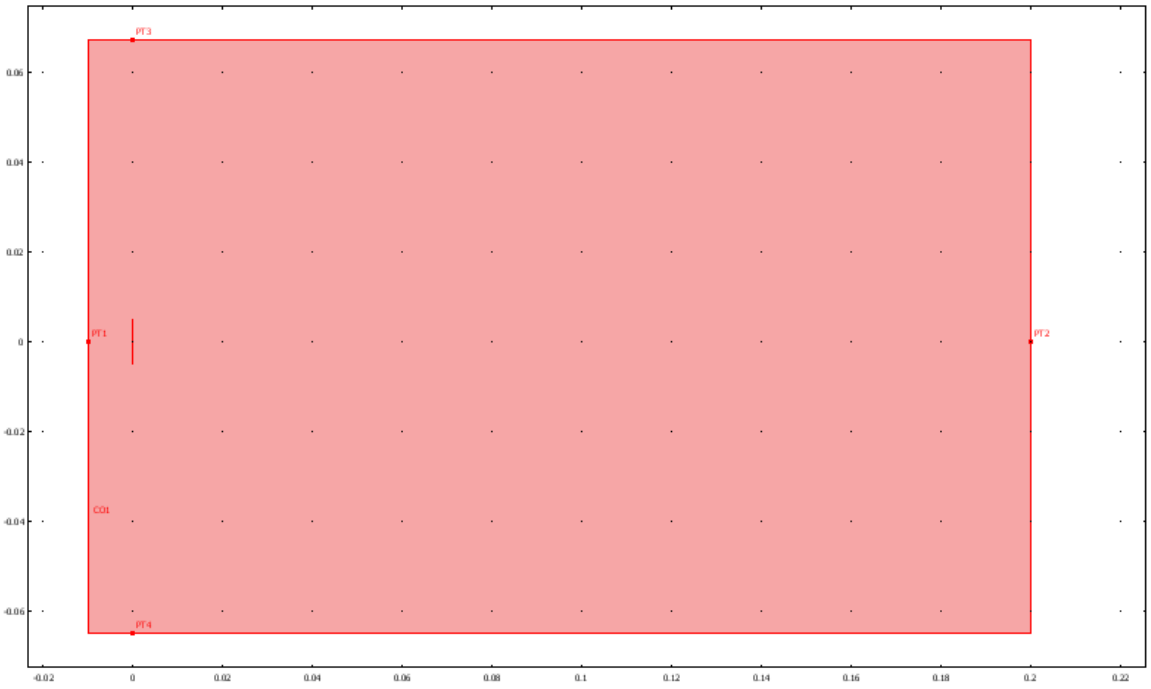
PT3
PT1
PT2
CO1
PT4
0.06
0.04
0.02
0
-0.02
-0.04
-0.06
-0.02
0
0.02
0.04
0.06
0.08
0.1
0.12
0.14
0.16
0.18
0.2
0.22

5.1.1. Point mode

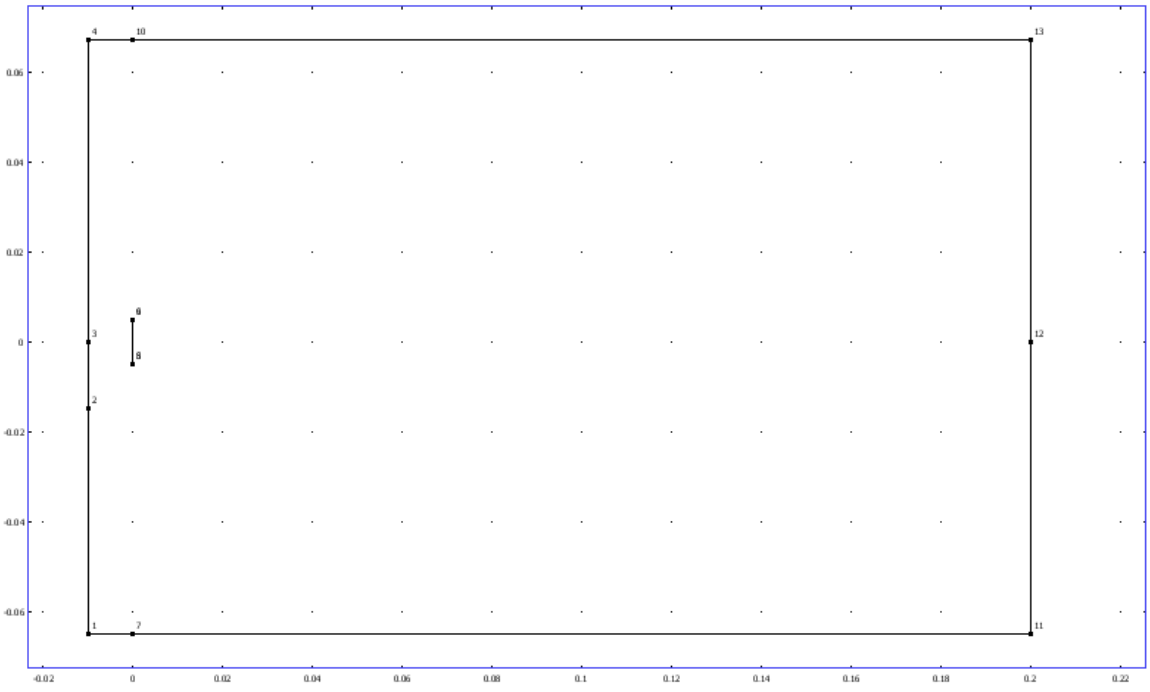

5.1.2. Boundary mode

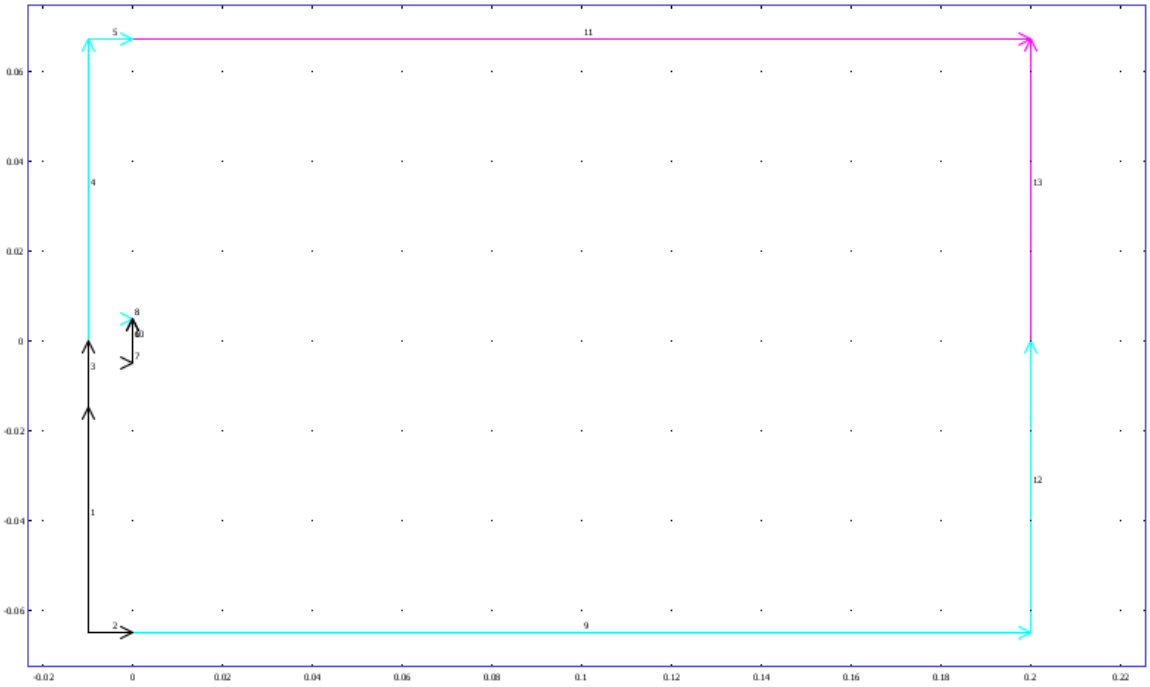

5.1.3. Subdomain mode

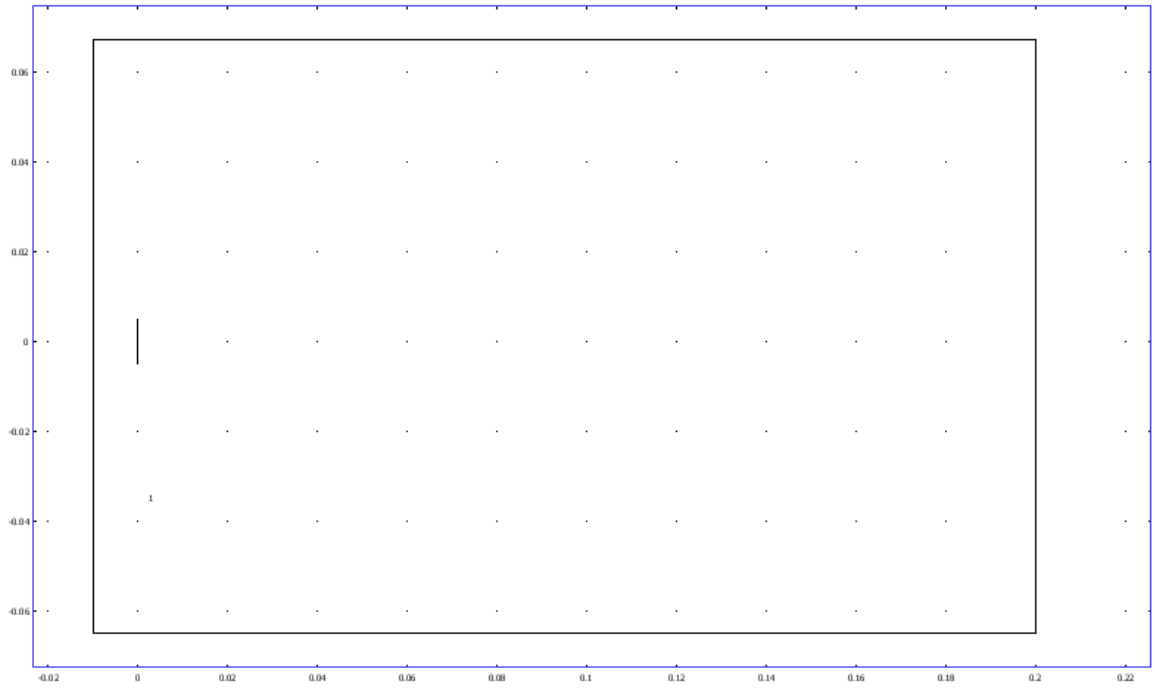

6. Geom1

The parameters and equations that govern the behavior of the anechoic chamber subdomain.

Space dimensions: 2D

Independent variables: x, y, z

6.1. Expressions

6.1.1. Boundary Expressions

The source is defined on boundary 10 (see Section A-5.1.2) It is entered in the Options>Expressions>Boundary Expressions field.

Boundary	10

source	wave

6.2. Mesh

The simulation mesh is defined based on the limiting parameters determined in the Constants section (Section A-3). They are entered in the Mesh>Free Mesh Parameters field under Custom mesh size>Maximum element size.

6.2.1. Mesh Statistics

Number of degrees of freedom	82256
Number of mesh points	20674
Number of elements	40908
Triangular	40908
Quadrilateral	0
Number of boundary elements	440
Number of vertex elements	13
Minimum element quality	0.7
Element area ratio	0.001

6.3. Application Mode: Pressure Acoustics (acpr)

Application mode type: Pressure Acoustics (Acoustics Module)

Application mode name: acpr

6.3.1. Scalar Variables

Name	Variable	Value	Description
p_i	p_i_acpr	exp(-.2*x)*sin(w0*t-k0*x)	Incident pressure wave
p_ref	p_ref_acpr	20e-6	Pressure reference

6.3.2. Application Mode Properties

Property	**Value**
Default element type	Lagrange - Quadratic
Analysis type	Transient
Damping	Off
Specify eigenvalues using	Eigenfrequency
Solve for	Total wave
Symmetry plane x=0	Off
Symmetry type for x=0	Symmetry
Symmetry plane y=0	Off
Symmetry type for y=0	Symmetry
Frame	Frame (ref)
Weak constraints	Off

6.3.3. Variables

Dependent variables: p

Shape functions: shlag(2,'p')

Interior boundaries not active

6.3.4. Boundary Settings

The boundary conditions are set. All boundaries are set to a perfect radiation condition except for the source. They are defined in the Physics>Boundary Settings field.

Boundary		1-3, 6-7	4-5, 8
Type		Radiation condition	Radiation condition
Pressure source (p0)	Pa	0	0
Wave direction (kdir)	1	{'-nx';'-ny'}	**{'-nx';'ny'}**

Boundary	9, 12	10	11, 13
Type	Radiation condition	Pressure	Radiation condition
Pressure source (p0)	0	**source**	0

Wave direction (kdir)	**{'nx';'-ny'}**	{'-nx';'-ny'}	**{'nx';'ny'}**

6.3.5. Subdomain Settings

The properties of the subdomain are set to the parameters for air. They are defined in the Physics>Subdomain Settings field.

Subdomain		1
Fluid density (rho)	kg/m^3	**rho_air**
Speed of sound (cs)	m/s	**c_air**

7. Solver Settings

Solve using a script: off

Analysis type	Transient
Auto select solver	On
Solver	Time dependent
Solution form	Automatic
Symmetric	auto
Adaption	Off

7.1. Direct (UMFPACK)

Solver type: Linear system solver

Parameter	**Value**
Pivot threshold	0.1
Memory allocation factor	0.7

7.2. Time Stepping

Using the minimum step size determined in the Constants section (Section A-3), the simulation parameters are set. They are defined in the Solve>Solver Parameters field.

Parameter	**Value**

Times	0:1.25e-7:1.5e-3
Relative tolerance	0.01
Absolute tolerance	0.0010
Times to store in output	Specified times
Time steps taken by solver	Free
Manual tuning of step size	Off
Initial time step	0.0010
Maximum time step	1.0
Maximum BDF order	2
Singular mass matrix	Maybe
Consistent initialization of DAE systems	Backward Euler
Error estimation strategy	Include algebraic
Allow complex numbers	Off

7.3. Advanced

Parameter	**Value**
Constraint handling method	Elimination
Null-space function	Automatic
Assembly block size	5000
Use Hermitian transpose of constraint matrix and in symmetry detection	Off
Use complex functions with real input	Off
Stop if error due to undefined operation	On
Type of scaling	Automatic
Manual scaling	
Row equilibration	On
Manual control of reassembly	Off
Load constant	On
Constraint constant	On
Mass constant	On
Damping (mass) constant	On
Jacobian constant	On
Constraint Jacobian constant	On

8. Postprocessing

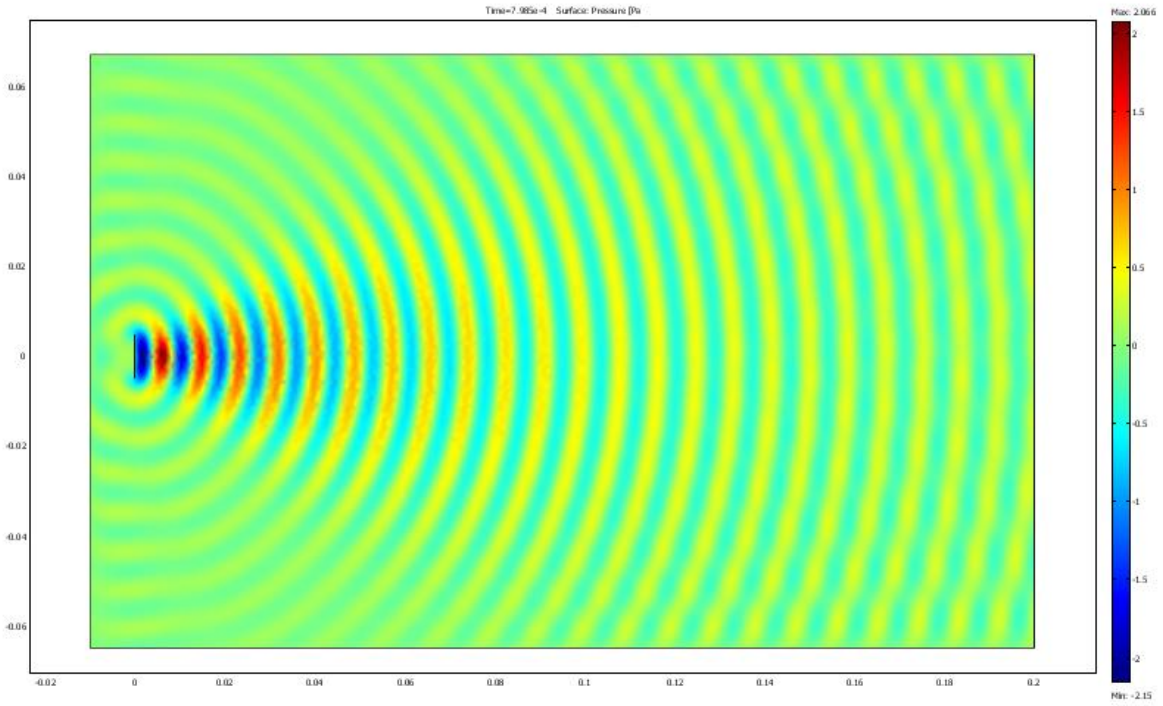

9. Variables

List of variables solved for during simulation.

9.1. Point

Name	Description	Expression
Lp_acpr	Sound pressure level	10 * log10(0.5 * p_t_acpr * conj(p_t_acpr)/p_ref_acpr^2)
Lp_s_acpr	Scattered sound pressure level	10 * log10(0.5 * p_s_acpr * conj(p_s_acpr)/p_ref_acpr^2)
p_t_acpr	Total acoustic pressure	p
p_s_acpr	Scattered pressure wave	p-p_i_acpr

9.2. Boundary

Name	Description	Expression
na_acpr	Normal acceleration	nx_acpr * ax_acpr+ny_acpr * ay_acpr
nk_acpr	Scalar product between n and kdir	(kdirx_acpr * nx_acpr+kdiry_acpr * ny_acpr)/sqrt(kdirx_acpr^2+kdiry_acpr^2)

9.3. Subdomain

Name	Description	Expression
ax_acpr	Local acceleration, x component	-(px-qx_acpr)/rho_acpr
ay_acpr	Local acceleration, y component	-(py-qy_acpr)/rho_acpr
Lp_acpr	Sound pressure level	10 * log10(0.5 * p_t_acpr * conj(p_t_acpr)/p_ref_acpr^2)
Lp_s_acpr	Scattered sound pressure level	10 * log10(0.5 * p_s_acpr * conj(p_s_acpr)/p_ref_acpr^2)
p_t_acpr	Total acoustic pressure	p
p_s_acpr	Scattered pressure wave	p-p_i_acpr
norma_acpr	Local acceleration, norm	sqrt(abs(ax_acpr)^2+abs(ay_acpr)^2)
normq_acpr	Dipole source, norm	sqrt(abs(qx_acpr)^2+abs(qy_acpr)^2)

Appendix B: Raw chamber data

Data measured in the anechoic chamber. Section B-1, Beam Axis Data, is data taken along the beam axis for longitudinal propagation; Section B-2, Lateral Propagation Data, is data taken perpendicular to the beam axis for lateral propagation characterization.

1. BEAM AXIS DATA							
D (in)	D(m)	Peak [dB]	Peak [Pa]				
7	0.1778	96.83348	1.39				
7.5	0.1905	96.71355	1.37				
8	0.2032	96.6413	1.36				
8.5	0.2159	96.5383	1.34				
9	0.2286	96.34799	1.31				
9.5	0.2413	96.27556	1.30				
12	0.3048	96.2363	1.30				
17	0.4318	96.09922	1.28				
35	0.889	95.02074	1.13				
59	1.4986	94.32261	1.04				
82.5	2.0955	93.82867	0.98				
2. LATERAL PROPAGATION DATA							
1.524m				.889m			
y (in)	y (m)	dB Peak	Pa Peak	y (in)	y (m)	dB Peak	Pa Peak
-3	-0.0762	90.7717	0.69	-3	-0.0762	89.5904	0.60
-2.5	-0.0635	91.8308	0.78	-2.5	-0.0635	91.1595	0.72
-2	-0.0508	91.9469	0.79	-2	-0.0508	92.4352	0.84
-1.5	-0.0381	92.7374	0.87	-1.75	-0.04445	92.955	0.89
-1.25	-0.03175	93.6766	0.97	-1.5	-0.0381	93.8804	0.99
-1	-0.0254	92.7868	0.87	-1.25	-0.03175	94.2965	1.04
-0.75	-0.01905	93.8607	0.99	-1	-0.0254	93.8512	0.99
-0.5	-0.0127	93.2477	0.92	-0.75	-0.01905	94.2604	1.03

0	0	94.3226	1.04	-0.5	-0.0127	94.2026	1.03
0.5	0.0127	93.2477	0.92	-0.25	-0.00635	94.647	1.08
0.75	0.01905	93.8607	0.99	0	0	95.0207	1.13
1	0.0254	92.7868	0.87	0.25	0.00635	94.647	1.08
1.25	0.03175	93.6766	0.97	0.5	0.0127	94.2026	1.03
1.5	0.0381	92.7374	0.87	0.75	0.01905	94.2604	1.03
2	0.0508	91.9469	0.79	1	0.0254	93.8512	0.99
2.5	0.0635	91.8303	0.78	1.25	0.03175	94.2965	1.04
3	0.0762	90.7717	0.69	1.5	0.0381	93.8804	0.99
				1.75	0.04445	92.955	0.89
				2	0.0508	92.4352	0.84
				2.5	0.0635	91.1595	0.72
				3	0.0762	89.5904	0.60

Appendix C: MatLab code

```
%PolyFit.m                                          Last edited 11/19/07


%Polynomial curve fit model for lateral propagation
%Equations and graphs for expected results of longitudinal propagation

clc; clear all; close all;

%CONSTANTS%**************************
c_air = 343;           %sound speed in air [m/s]
rho_air = 1.205563;    %density of air [kg/m^3]
f=40000;               %frequency of source [hz]
w0 = 2*pi*f;           %radial frequency of source [rad/s]
Po = 2;                %initial pressure of source [Pa]
lamda = c_air/f;       %wavelength of source [m]
k = (2*pi)/lamda;      %wavenumber of source
w = 2*pi*70;           %lateral spread frequency

%for calculating alpha:
mu = 18.27E-6;          %viscosity [Pa/s]
mub = .6*mu;            %bulk viscosity
Vsquig = (4/3) + mub/mu;    %viscosity number
v = mu/rho_air;         %kinematic viscosity coefficient
sigv = (w0*v)/c_air^2;  %dimensionless coefficient
Cp = 1.012*1000;        %specific heat at constant pressure [J/(kg*K)]
gamma = 1.4;            %ratio of specific heats
kh = .025;              %heat conduction coefficient
Pr = mu*Cp/kh;          %Prandtl number
alpha = ((w0^2*v)/(2*c_air^3))*(Vsquig + (gamma-1)/Pr);
%yields alpha = .0293, 2% off of graph value of alpha at 0% h
%************************************

%VARIABLES%**************************
t  = .81;               %0:.001E-3:1.9E-3;
y =-.065:.0001:.065;    %lateral distance
x =.1522; %0:.0001:.5;  %distance along beam axis
%************************************

%FUNCTIONS%**************************
chamberDecay = (Po)*exp(-.196*x);  %Expected Results for Peak Decay

peakDecay = Po*sin(w0*t-k*x).*exp(-.196*x).*(1/x.^.5);
%Computer model decay
lateralDecay = 928117*y.^6 + 4E-5*y.^5 - 8697.2*y.^4 + 8E-7*y.^3 -
4.8533*y.^2 + 5E-9*y + peakDecay;
lateralPoly = 1E2*y.^4 + 50*y.^3 + 2000*y.^2 - .1*y+1;
lateralCos = -.005*cos(w*y).*lateralPoly;
lateralSpread = lateralDecay + lateralCos;
```

```
%***********************************

%CURVE FITS%*************************
peakDecay1m = Po*sin(w0*(.75013)-k*(.1025)).*exp(-.196*(.1025));
%Computer model decay
lateralDecay1m = 1E6*y.^6 + 3E-5*y.^5 + 2907.6*y.^4 + 2E-6*y.^3 -
121.83*y.^2 + 4E-10*y + peakDecay1m;
lateralPoly1m = 1E2*y.^4 + 50*y.^3 + 2000*y.^2 - .1*y+1;
lateralCos1m = .005*cos(2*pi*80*y).*lateralPoly1m;
lateralSpread1m = lateralDecay1m + lateralCos1m;
%***********************************

%PLOTTING%***************************
plottools ON;
figure(1);
plot(y,lateralSpread, y, lateralSpread1m);

figure(2);
plot(y,lateralDecay);

figure(3);
plot(y, lateralPoly);

figure(4);
plot(y, lateralCos);

figure(5);
plot(x, peakDecay);
%***********************************
```

```
%HermiteGaussianFit.m                          Last edited 11/19/07

%Hermite-Gaussian and Hermite Polynomial curve fits

clc; clear all; close all;

%CONSTANTS%*************************
n=6;
m=20;
o=14;
c_air=343;
freq=40000;
w0=2*pi*freq;
k0=w0/c_air;
Po=2;
lambda=c_air/freq;
y=-.08:.00001:.08;
```

```
x=1.526;
t=.75013;  %0:.01e-3:1e-3;
%**********************************

%FUNCTIONS***************************
deriv = nthDeriv(n);           %nth deriv of the hermite polynomial
derivm = nthDeriv(m);          %mth deriv of the hermite polynomial
derivo = nthDeriv(o);          %oth deriv of the hermite polynomial

Herm=polyval(deriv,y)*(-1^n);  %makes graphable poly from nth deriv
HermM=polyval(derivm,y/.008)*(-1^m);
Hermo=polyval(derivo,y/.008)*(-1^o);

Gaus=exp((-(y).^2)/2);         %gaussian portion
GausShrink=exp((-(y/.075).^2)/2);   %rescaling the functions
GausSuperShrink = 1E-9*exp((-(y/.01).^2)/2);

HGn = GausShrink.*Herm*.023-.345;  %Hermite Gaussian polynomial
normalized
HGm=Gaus.*HermM;               %to zero, and various tests of different
HGo=Gaus.*Hermo;               %combinations for best fit
Hsq=Herm.*HermM;
Hcub=Hsq.*Hermo;
%**********************************

%CURVE FIT FUNCTIONS%*****************
%0.1m HG fit:
centerVar1m = cos(2*pi*10019.75*.75013-(2*pi*10019.75/343)*x-39205.5);
HermM1m =polyval(derivm,y/.009)*(-1^m);
GausSuperShrink1m = 1E-9*exp((-(y/.0126).^2)/2);
AShrink1m = 25*y.^2 +.005;
GausShrink1m =exp((-(y/.04).^2)/2);
HGn1m = GausShrink1m.*Herm*.06;
longitudeWave1m = Po*sin(w0*.75013-k0.*.1025).*exp(-
.197.*.1025).*(1./(11.31*(.1025.^.5)));
%along beam axis
SinVar1m = HermM1m.*GausSuperShrink1m.*AShrink1m.*centerVar1m;
HlateralSpread1m = [SinVar1m+HGn1m+.1].*longitudeWave1m;

%0.15m HG fit:
centerVar15 = cos(2*pi*10019.75*.75013-(2*pi*10019.75/343)*.1539-
39205.5);
HermM15=polyval(derivm,y/.0084)*(-1^m);
GausSuperShrink15 = 1E-9*exp((-(y/.0099).^2)/2);
AShrink15 = 740*y.^2+.02;
HGn15 = GausShrink.*Herm*.06;
longitudeWave15 = Po*sin(w0*.75013-k0.*.1539).*exp(-
.197.*.1539).*(1./(12.65*(.1539.^.5)));
SinVar15= HermM15.*GausSuperShrink15.*AShrink15.*centerVar15;
HlateralSpread15 = [SinVar15+HGn15+.1]*longitudeWave15;
```

```
%measured data HG fit:
centerVarMe = cos(2*pi*10019.75*.75013-(2*pi*10019.75/343)*x-39204.2);
HermoMe=polyval(derivo,y/.00999)*(-1^o);
GausSuperShrinkMe = 1E-5*exp((-(y/.0115).^2)/2);
AShrinkMe = 70*y.^2+.04;
GausShrinkMe = exp((-(y/.085).^2)/2);
HGnMe = GausShrinkMe.*Herm*.06+.07;
longitudeWaveMe = Po*sin(w0*t-k0.*x).*exp(-.197.*x)-.441;
SinVarMe = HermoMe.*GausSuperShrinkMe.*AShrinkMe.*centerVarMe;
HlateralSpreadMe = [SinVarMe+HGnMe-.02]*longitudeWaveMe;
%**********************************

%PLOTS*****************************
figure(1);
plot(x, centerVarMe);
figure(2);
plot(y, AShrinkMe);
figure(3);
plot(y, SinVarMe);
figure(4);
plot(y, HGnMe);
figure(5);
plot(y, HlateralSpreadMe);
%**********************************
```

```
%HermiteDeriv.m                                    Last edited 11/19/07

%This function takes a polynomial u and returns du/dx-u*x.  This is
%for deriv[u*exp(-x^2/2)] = [du/dx-u*x]*exp(-x^2/2).  A loop will have
%to be created in the calling function to find the nth deriv.

function Un=HermiteDeriv(u)

%CONSTANTS%*************************
zero = [0];
x=[1 0];
%**********************************

%VARIABLES%*************************
%**********************************

%FUNCTIONS*************************
  u1=polyder(u); % du/dx
  a=conv(u,x);   % u*x
  aLength = size(a);  % length of a matrix
  u1Length = size(u1); % length of u1 matrix
  extra0 = aLength-u1Length;  % difference between lengths
```

```
  zeroFill = repmat(zero,1,extra0(1, 2));  % zero matrix of length extra0
for padding
  u1Pad = [zeroFill,u1];      %u1 now same size as a
  Un = u1Pad-a;
%************************************
```

%nthDeriv.m **Last edited 11/19/07**

```
%returns the nth derivative of exp[(-x^2)/2]

function Nderiv = nthDeriv(n)

%CONSTANTS%**************************
u=[1];
%************************************

%VARIABLES%**************************
m=1:1:n;
%************************************

%FUNCTIONS%**************************
for i=1:length(m)
    Nderiv = HermiteDeriv(u);
    u = Nderiv;
end
%************************************
```